NLRP3 INFLAMMASOME CONTRIBUTES TO RETINAL GANGLION CELL (RGC) DEATH IN THE DBA/2J MOUSE MODEL OF GLAUCOMA

by

Siqi Li

B.Sc, Zhejiang University, 2017

A THESIS SUBMITTED IN PARTIAL FULFILLMENT OF THE REQUIREMENTS FOR THE DEGREE OF

MASTER OF SCIENCE

in

The Faculty of Graduate and Postdoctoral Studies

(Cell and Developmental Biology)

THE UNIVERSITY OF BRITISH COLUMBIA

(Vancouver)

September 2020

The following individuals certify that they have read, and recommend to the Faculty of Graduate and Postdoctoral Studies for acceptance, a thesis entitled:

NLRP3 INFLAMMASOME CONTRIBUTES TO RETINAL GANGLION CELL (RGC) DEATH IN THE DBA/2J MOUSE MODEL OF GLAUCOMA

submitted by Siqi Li in partial fulfillment of the requirements for

the degree of Master of Science

in Cell and Developmental Biology

Examining Committee:

Joanne Matsubara, Cell and Developmental Biology
Supervisor

Orson Moritz, Cell and Developmental Biology
Supervisory Committee Member

Tim O'Connor, Cell and Developmental Biology
Supervisory Committee Member

Deborah Giaschi, Department of Ophthalmology and Visual Sciences
Additional Examiner

Additional Supervisory Committee Members:

Elizabeth Simpson, Department of Medical Genetics
Supervisory Committee Member

Abstract

Glaucoma is a neurodegenerative eye disease characterized by elevated intraocular pressure (IOP) in the majority of cases, followed by retinal ganglion cell (RGC) loss. Neuroinflammation is an important factor contributing to RGC death during glaucoma pathogenesis. Evidence suggests that NLRP3 (nucleotide-binding oligomerization domain (NOD)-like receptor protein 3) inflammasome activity is associated with IOP-induced RGC death.

To investigate whether NLRP3 inflammasome is activated by IOP elevation, the DBA/2J mouse model of glaucoma with age-related IOP elevation was studied. Female mice were sacrificed at 3 or 9 months of age. IOP was measured before sacrifice. NLRP3 inflammasome related proteins and RGC loss were quantified in eye tissues. To further assess whether NLRP3 inflammasome activation contributes to RGC death, mice were treated with 8 weeks of daily oral administration of 30 mg/kg MCC950, a specific small-molecule drug that prevents NLRP3 inflammasome activation.

In the 9-month DBA/2J mice, IOP was significantly increased compared to 3-month mice. Concomitantly, protein levels of NLRP3 and cleaved caspase-1 were significantly higher in 9- month DBA/2J. The plasma level of circulating MCC950 (7650±775.3 ng/ml) after 8 weeks of drug administration was above the efficacy threshold (>1000 ng/ml). The MCC950 treated mice retained a higher number of surviving RGCs, exhibited lower levels of NLRP3 expression and caspase-1 cleavage compared to age-matched controls.

In this study, we discovered MCC950 treatment inhibits the age-related increase of NLRP3 inflammasome activity and ameliorates RGC loss, suggesting that NLRP3 inflammasome activation is associated with RGC death in this mouse model.

Lay Summary

Glaucoma is a group of eye diseases characterized by the loss of important neurons in the retina responsible for vision. Previous studies suggest the damage is possibly due to a protein complex called “inflammasome.” We used a mouse model that mimics glaucoma symptoms and detected the inflammasome level within the mouse eye. We found that the level of inflammasome proteins is significantly increased with age and elevated eye pressure. We also used a drug called “MCC950” to treat the animals, which prevented the activity of inflammasome protein complex, and thereby protected the retinal ganglion cells (RGCs). This study demonstrated the role of the inflammasome protein complex in a mouse model of glaucoma, and identified a way to inhibit inflammasome activity within the mouse eye. These findings bring insight into RGC death during glaucoma disease progression, and a possible method to suppress RGC death by inhibiting the activation of the inflammasome.

Preface

I designed, performed, and analyzed all experiments within this thesis under the supervision of Dr. Joanne Matsubara. Dr. Jing Cui assisted with animal anesthetization, IOP measurement and whole-mount preparation. Aikun Wang assisted with protein lysate extraction, and Hans Adomat at Vancouver Prostate Centre helped with MCC950 concentration analysis.

The following data presented in Chapter 3 is currently being prepared for a journal submission.

All *in vivo* experiments were approved by the UBC Animal Care Committee protocols A17-0229 listed under principal investigator Dr. Joanne Matsubara

- Figure 1.1 is reprinted from JAMA, 311(18); Weinreb, Robert N.; Aung, Tin, The Pathophysiology and Treatment of Glaucoma: A Review, 1901-1911, Copyright (2014), with permission from American Medical Association.
- Figure 1.2 is reprinted from Fu, Xin; Huu, Viet Anh Nguyen, Clinical applications of retinal gene therapies, Precision Clinical Medicine, 2018, Vol 1, Issue 1, Pages 5-20, by permission of Oxford University Press
- Figure 1.3 is adapted from Soto I, Howell GR. The complex role of neuroinflammation in glaucoma. Cold Spring Harb Perspect Med. 2014;4(8):a017269. Published 2014 Jul 3. doi:10.1101/cshperspect.a017269
- Figure 1.4 is reprinted from Song, Limin, et al. "NLRP3 inflammasome in neurological diseases, from functions to therapies." Frontiers in cellular neuroscience 11 (2017): 63.

- Figure 1.5 is reprinted from Trends in Biochemical Sciences, 41(12), Yuan He, Hideki Hara, Gabriel Núñez, Mechanism and Regulation of NLRP3 Inflammasome Activation, 1012-1021, Copyright (2016), with permission from Elsevier.

Table of Contents

List of Tables

List of Figures

List of Abbreviations

ABC	Avidin biotin complex
AIM2	Interferon-inducible protein absent in melanoma 2
ACN	Acetonitrile
ASC	Apoptosis-associated speck-like protein containing CARD
BCA	Bicinchoninic acid
BHB	body β- hydroxybutyrate
BRB	Blood-retina-barrier
CARD	Caspase activation and recruitment domain
CDR	Cup-to-disc ratio
CNS	Central nerve system
CT	C-terminal
DAMP	Damage/danger-associated molecular pattern
FFPE	Formalin-fixed paraffin embedded
FLICA	Fluorochrome Inhibitor of Caspases assay
GAPDH	Glyceraldehyde 3-phosphate dehydrogenase
GCL	ganglion cell layer
GDI	Glaucoma drainage implant
GDP	Glaucoma discovery platform
GSDMD-NT	Gasdermin D N-terminal
GSDMD-CT	Gasdermin D C-terminal
HMGB1	High mobility group box 1
IF	Immunofluorescent

IHC	Immunohistochemistry
IL-1β	Interleukin-1 beta
IL-18	Interleukin-18
INL	Inner nuclear layer
IOP	Intraocular pressure
IPD	Iris pigment dispersion
IPL	Inner plexiform layer
ISA	Iris stromal atrophy
LRR	Leucin-rich repeat
NACHT	[NAIP (neuronal apoptosis inhibitory protein), CIITA (MHC class II transcription activator), HET-E (incompatibility locus protein from Podospora anserina) and TP1 (telomerase-associated protein)]
NF-kB	Nuclear factor kappa-light-chain-enhancer of activated B cells
NLR	Nucleotide-binding oligomerization domain-like receptor
NLRP1	Nucleotide-binding oligomerization domain-like receptor protein 1
NLRP3	Nucleotide-binding oligomerization domain-like receptor protein 3
NLRC4	NOD-like receptor containing a CARD 4
NOD	nucleotide-binding oligomerization domain
NT	N-terminal
NTG	Normal tension glaucoma
OCT	Optical coherence tomography
ONH	Optic nerve head

ONL	Outer nuclear layer
OPL	Outer plexiform layer
P2X7	P2X purinoceptor 7
PACG	Primary angle-closure glaucoma
PAMP	Pathogen-associated molecular pattern
Panx1	Pannexin-1
PBS	Phosphate buffered saline
PDS	Pigmentary dispersion syndrome
POAG	Primary open-angle glaucoma
pONC	Partial optic nerve crush
PPD	Paraphenylenediamine
PR	Purinergic receptors
PRR	Pattern recognition receptor
PVDF	Polyvinylidene difluoride
PYD	Pyrin domain
RGC	Retinal ganglion cell
RIPA	Radioimmunoprecipitation assay
RNFL	Retinal nerve fiber layer
ROS	Reactive oxygen species
RPE	Retinal pigment epithelium
RT	Room temperature
SEM	Standard error of the mean
SR	Scavenger receptors

T2D	Type 2 diabetes
TBS	Tris-buffered saline
TLR	Toll-like receptor
TM	Trabecular meshwork
TNF-α	Tumor necrosis factor-α
TRPV4	Transient receptor potential vanilloid isoform 4
UPLC	Ultra-performance liquid chromatography

Acknowledgements

I would like to give my special thanks to Dr. Joanne A. Matsubara for the guidance and endless support to my thesis work and study as a graduate student. In the past two years your countless patient guidance and encouragement have got me through many failed experiments. I'm truly grateful for all the help you've given me all the time. I would also like to thank members at my supervisory committee, Dr. Orson Moritz and Dr. Elizabeth Simpson for the kind help and input into my thesis work. Your comments at each meeting were a great help in directing me in the thesis study. And I would like to extend my thanks to Dr. Tim O'Connor for your input into my thesis writing and presentations. Importantly, I would like to give my thanks to all the lab members, especially to Dr. Jing Cui and Dr. Jiangyuan Gao, who have given me great help in experiments and in many other aspects in life. Lastly special thanks to my parents, friends and partner, your encouragement and support have helped me through countless hard times.

Dedication

I dedicate this thesis to my parents, I appreciated their unconditional support during my life and in my studies. I'm always grateful for the love and education they've given me for my entire life. And I would like to give this special thank to my lovely partner, who's always by my side and encouraging me throughout my student life as a graduate student.

Chapter 1: Introduction

1.1 Overview of Glaucoma

1.1.1 What is Glaucoma?

Glaucoma is one of the leading causes of vision impairment and irreversible blindness.[1] It affects more than 70 million individuals worldwide and approximately 10% of them are bilaterally blind.[2-3] The prevalence of glaucoma is rapidly increasing. An estimated 111.8 million people will be affected by 2040 according to a meta-analysis.[4] The main cause of glaucoma is intraocular hypertension. High intraocular pressure (IOP) could cause mechanical stress to the posterior structure of the eye and damage the optic nerve along with their cell bodies, the retinal ganglion cells (RGCs). If left untreated, glaucoma could gradually progress from mild to severe visual impairment and subsequently lead to blindness.[5] Studies suggest that the laminar cribrosa at the optic nerve head (ONH, where the RGC axons leave the eye) may undergo severe mechanical damage, as it is one of the weakest points of a hypertensive eye. This may result in deformation and remodelling of the laminar cribrosa,[6] and subsequent damage of the axons and interruption of the retrograde delivery of essential factors to the RGCs.[2]

In the majority of glaucomatous eyes, hypertension is caused by the accumulation of aqueous humor. Aqueous humor is generated by the ciliary processes, it flows through the anterior chamber and drain out through the trabecular meshwork (TM) (Figure 1.1). The secretion of aqueous humor and regulation of its outflow are important in maintaining IOP.[7] In glaucomatous eyes, the outflow resistance increases, and the generation/drainage of the aqueous humor becomes imbalanced, thereby leading to elevated IOP.

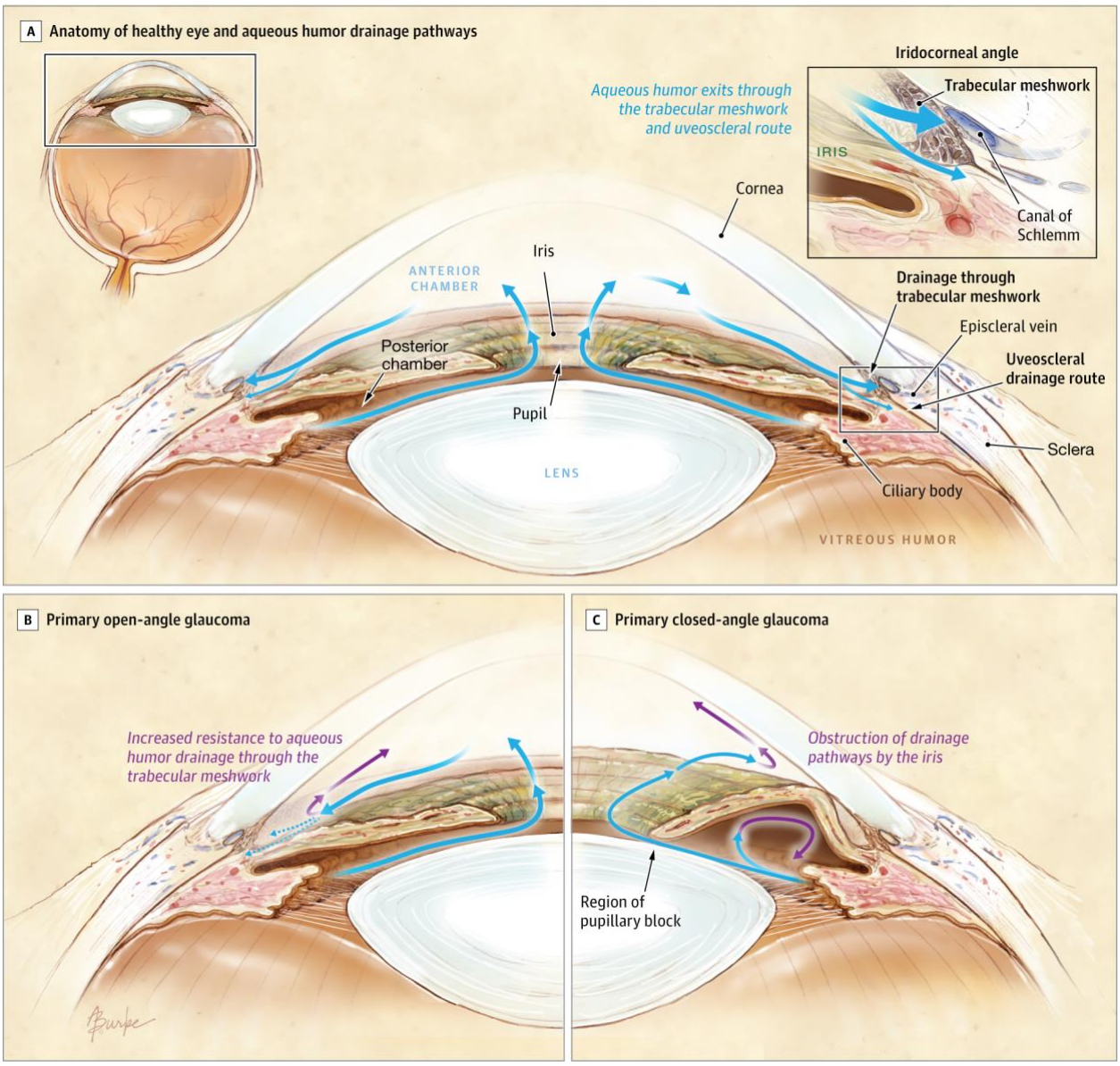

Figure 1.1 Aqueous humor drainage pathways of healthy and glaucomatous eyes. In normal eyes aqueous humor is generated by the ciliary body and drains out through the trabecular meshwork to the episcleral veins (A, blue arrow indicates aqueous humor flow). In primary open-angle glaucoma (POAG), the aqueous humor is accumulated due to the increased resistance of the trabecular meshwork (B), while in primary angle closure glaucoma (PACG, or primary closed-angle glaucoma) the iris is abnormally positioned and obstruct the outflow of aqueous humor (C).
Reprinted from Weinreb RN, Aung T, Medeiros FA. The Pathophysiology and Treatment of Glaucoma: A Review. JAMA. 2014;311(18):1901–1911. doi:10.1001/jama.2014.3192.

1.1.2 Classification of glaucoma

Glaucoma is classified in different ways based on the disease progression time and pathological factors. Each type of glaucoma is unique, and they are generally divided into two major categories: primary glaucoma and secondary glaucoma.

Primary glaucoma includes primary open angle glaucoma (POAG), primary angle closure glaucoma (PACG) and normal tension glaucoma (NTG). Both POAG and PACG are characterized by elevated IOP caused by the imbalanced flow of aqueous humor, while NTG is optic nerve damage without ocular pressure exceeding normal range.

In POAG eyes, the iris and cornea remain in normal position with an open angle (Figure 1.1 B). The blocked drainage of aqueous humor is caused by a high-level of resistance in the trabecular meshwork. It is the most common type of glaucoma accounting for 74% of all glaucoma cases,[3] and is predominant among Caucasians and Africans.[8-9] Although POAG eyes may not show symptoms at the beginning of the disease process, the optic nerve is gradually damaged overtime, which affects the vision as well. Unfortunately, the damage cannot be reversed in current glaucoma disease treatment, and early diagnosis cannot be easily achieved due to the mild symptoms.

PACG, also named narrow-angle glaucoma, it is characterized by an anatomical disorder of the anterior segment of the eye.[10] In PACG, the outflow pathway is obstructed by the abnormally positioned iris, which forms a narrow angle with the cornea and closes the anterior chamber (Figure 1.1 C). PACG can be chronic or acute. Acute PACG may be caused by a sudden and dramatic dilation of the pupil. Hypertension builds up quickly in acute PACG eyes, along with the occurrence of severe pain and redness in the eye. If left untreated, acute PACG can cause blindness within a few days. Chronic PACG progresses more slowly and may not have

any symptoms. The cause of chronic PACG is still unclear, with multiple potential causes that could lead to gradually closing of the drainage angle, including a large lens or an iris that is thicker than normal.[11]

In some cases, glaucomatous neuropathy occurs in the eye with normal intraocular pressure, and these are classified as normal-tension glaucoma. The "normal tension" results in axon damage and laminar cribrosa disorders, and these may be due to the impaired low cerebrospinal fluid pressure in optic nerve sheath compartment,[12] vascular dysregulation or hypersensitivity to the normal pressure.[13] Further studies are required to better understand the mechanism behind NTG, and in spite of the alternative cases, hypertension is still the major contributor to glaucomatous neuropathies.

Secondary glaucomas are glaucomas that are caused by other acquired conditions, such as trauma, certain medications, uveitis,[14] or post-surgical complications.[2] Pigmentary glaucoma is one of the secondary glaucomas, characterized by pigmentary dispersion syndrome (PDS). The dispersed pigments, originating from a degenerative iris, precipitates at the anterior segment of the eye, which blocks the drainage of the aqueous humor and results in IOP elevation. In most cases PDS is associated with an iris trans-illumination defect, being more obvious in light-colored eyes.[15] The mouse strain (DBA/2J) used in this study is an animal model of pigmentary glaucoma, discussed in detail in section 1.4. Secondary glaucoma also includes neovascular glaucoma, exfoliation glaucoma and uveitic glaucoma.[16-17]

1.1.3 Diagnosis of glaucoma

Glaucomatous structural damage can be assessed by examination of optic nerve head (ONH) and retinal nerve fiber layer (RNFL). Traditional method of diagnosis is through

gonioscopy, which uses a goniolens and an operating microscope to view the anatomical angle formed between the cornea and iris. However, given the subjectiveness and low repeatability of gonioscopy, the diagnosis of glaucoma now is routinely assessed by optical coherence tomography (OCT), which examines the morphological changes of the optic nerve caused by glaucoma.[2] The ONH exhibits a cup-to-disc ratio (CDR): the "cup" is the central area of the ONH where the optic nerves and blood vessels enter the retina; the "disc" stands for optic disc, which is another name of the ONH. A high CDR of more than 0.3 normally indicates glaucoma symptoms. The average RNFL thickness can also be detected through OCT imaging,[18] lower thickness indicates RGC loss and reduction in RGC neuronal density.

1.1.4 Treatment of glaucoma

IOP-lowering medications in eye drop formulation, have been used widely in POAG management, and can be divided into 5 major classes: prostaglandin analogues, beta-blockers, diuretics, cholinergic agonists, and alpha agonists.[19] Prostaglandin analogues are a class of drugs that bind to prostaglandin receptors on the cell surface; they can reduce IOP by decreasing the outflow resistance at TM, thereby reducing the cumulative aqueous humor in the anterior chamber. The mechanism underlying beta-blockers is complementary to prostaglandins, as beta-blockers reduce the generation of aqueous humor from ciliary bodies. However, they may cause cardiac or respiratory side effects. Recently a new type of reagent has emerged, known as rho kinase inhibitors. The rho kinase inhibitors can act directly on the contractile tone of TM and increase the outflow.[20]

Given that the medical management of ocular hypertension does not work on all patients, there are laser and surgical treatments for glaucoma. Typical laser treatment is by argon laser

trabeculoplasty, which produce thermal changes to the TM that increases the outflow of aqueous humor. Surgical treatment is by far the most invasive strategy and is mainly chosen when both medication and laser trabeculoplasty fail. Surgical methods include glaucoma drainage implants (GDIs) and trabeculectomy, which surgically removes a portion of TM.

Current treatment strategies for glaucoma still have their disadvantages and concerns. For IOP-lowering drops, patients are required to take the medication daily, however patient compliance is a concern and remains a challenge. Furthermore, eyedrops are successful in lowering elevated IOP in only 39% of those who choose this treatment.[21] The eyedrops also have various side-effects, including irritation of the ocular surface, eye redness, headache, etc.[22] Some of the glaucoma eyedrop medications can even result in toxicity to cornea.[23] Furthermore, in addition to all the disadvantages of eyedrop treatments, simply lowering IOP does not reverse RGC loss if it has already occurred.

Surgical treatments for lowering IOP are highly invasive and are usually accompanied by various complications. There are short-term and long-term complications after surgical treatment, including hyphema, choroidal effusions, and chorioretinal detachment.[24] Elderly patients may also have a higher risk of cataracts after surgery.[25] Therefore, developing new treatment strategies targeting glaucomatous symptoms and rescuing RGCs are of great importance.

1.2 Overview of pathogenesis of glaucoma

1.2.1 Risk factors of glaucoma

There are several risk factors for glaucoma, and aging is one of the most important factors.[26] Studies and meta-analysis have proved that glaucoma is a neurodegenerative disorder

strongly associated with increased age.[27] The estimated prevalence of glaucoma among those aged 40-80 is 3.54% worldwide.[4] Glaucoma in the elderly may possibly be associated with an increased risk of Alzheimer's disease[28] linked by the their shared characteristics: progressive neurodegeneration and chronic microvascular insults.[29]

The risk factor that is considered to contribute the most to glaucoma is increased IOP. Elevated IOP that exceeds retinal perfusion pressure results in retinal ischemia, inadequate blood supply, and RGC death. Inflammation could occur in response to ischemic injury induced by elevated IOP. The exact mechanisms of IOP-induced RGC cell death are not well understood, and some studies suggest that retinal immune cells initiate inflammatory responses, and produce pro-inflammatory factors, which lead to subsequent apoptosis of RGCs.[30]

1.2.2 The anatomy structure of retina

The retina, a part of the central nervous system (CNS), is a multilayered structure comprised of RGCs and many other types of retinal cells (Figure 1.2). From the innermost to the outermost, the retina is divided into multiple layers as following: The nuclei of ganglion cells form the ganglion cell layer (GCL) that lies innermost in the retina, which is also closest to the lens and front of the eye. The inner plexiform layer (IPL) lies next to GCL, it contains the synapse between dendrites of RGCs, amacrine cells and bipolar cell axons. The inner nuclear layer (INL) lies next to IPL, containing the nuclei of amacrine cells, bipolar cells and horizontal cells. The following outer plexiform layer (OPL) contains the projections of photoreceptors (rods and cones) and their synapses with bipolar cells and horizontal cells. The outer nuclear layer (ONL) consists cell bodies of rods and cones. The outer most layer of the retina only consists of a single layer of epithelium cells known as retinal epithelium cell (RPE). [31]Light travel through

the thickness of retina and activate photoreceptors, where the absorption of photons is converted into biochemical signals and then electrical signals. The retinal messages then are transmitted into the brain through RGCs and optic nerves. Glaucoma is known to cause progressive RGC loss, and studies demonstrated that glaucomatous damage may involve structural change in the photoreceptor layer as well.[32]

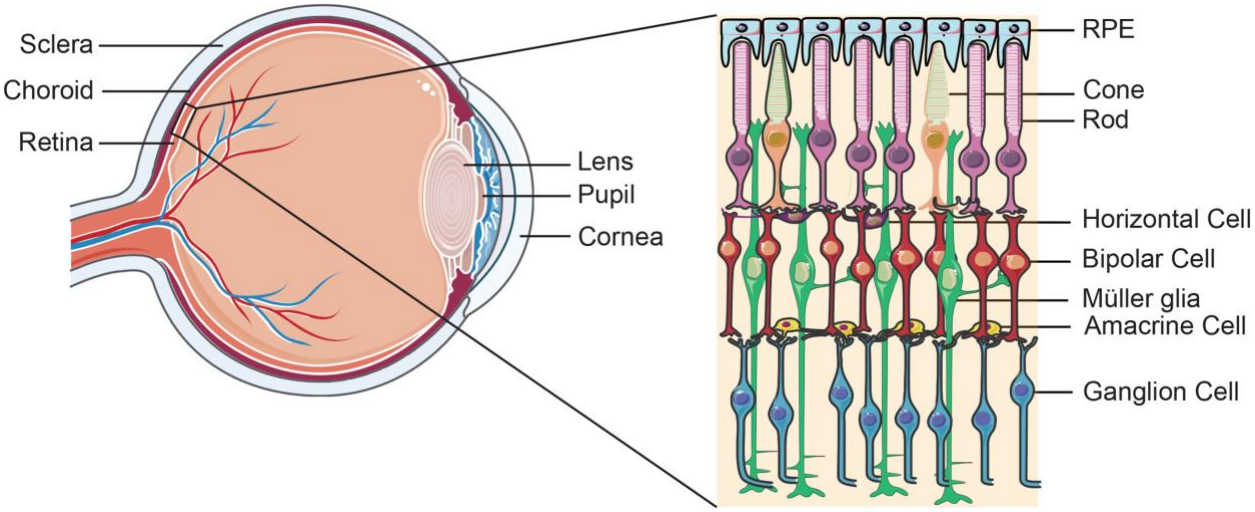

Figure 1.2 Schematic of the eye and retina structure. The magnified area represents different cell types in the retina. Retinal ganglion cells (RGCs) are located at the innermost layer of the retina.
Reprinted from Xin Fu, Viet Anh Nguyen Huu, Yaou Duan, Daniel S Kermany, Carolina C S Valentim, Runze Zhang, Jie Zhu, Charlotte L Zhang, Xiaodong Sun, Kang Zhang, Clinical applications of retinal gene therapies, Precision Clinical Medicine, Volume 1, Issue 1, June 2018, Pages 5–20

Central retina is considerably thicker than peripheral retina due to the increased packing density of photoreceptors and RGCs/bipolar cells compared to peripheral retina. The difference in thickness is mainly in the difference of GCL and IPL. The central retina has a greater number of RGCs associated with bipolar cells and photoreceptors, which also means more synaptic interaction in the thicker IPL and greater numbers of ganglion cell axons coursing to the optic nerve in the nerve fiber layer.[33]

1.2.3 Neuroinflammation in glaucoma – astrocytes and microglia

Neuroinflammatory responses in CNS have been widely observed in the glaucomatous eye tissues, suggesting an important role of inflammation in chronic glaucoma.[34] Evidence suggests that early neuroinflammatory responses at the ONH could be the mechanism behind RGC axon damage in glaucomatous eyes.[35-36] Also, ocular hypertension could induce neuroinflammation in the optic nerve and retina by introducing mechanical stress and ischemic injury.[37] Therefore, the role of inflammation in neurodegeneration of the retina associated with elevated IOP is of great interest.

The eye has a special relationship with the immune system known as "immune privilege", which means that the eye could tolerate the antigen invasion without triggering the inflammatory immune response mediated by macrophages. In the eye, immune privilege is maintained by a physical barrier called the blood-retina barrier (BRB).[38] BRB was once believed to prevent immune cell infiltration and form "immune-ignorance" in the eye. However in the past few years, studies have demonstrated that instead of a complete suppression of the immune response, the privilege of immune system in the eye is a type of selective and regulated immune response.[39-40] Inflammatory responses could be characterized and mediated by multiple cells, especially the resident innate immune cells in CNS -- astrocytes and microglia cells. (Figure 1.3)

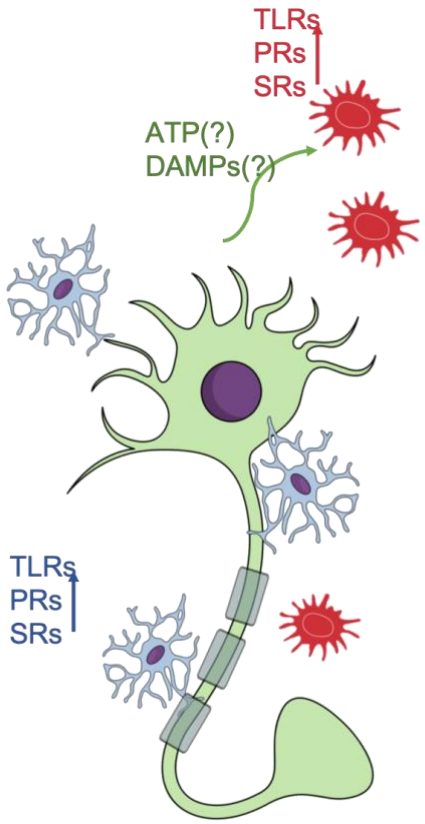

Figure 1.3 Inflammatory responses in the CNS are mediated by resident astrocytes and microglia. The immune system in CNS comprises neurons (green), astrocytes (blue, with processes) and microglia (red, with processes) that sense environmental changes. Glial cells (astrocytes and microglia) express pattern recognition receptors (PRRs) such as toll-like receptors (TLRs), purinergic receptors (PRs) and scavenger receptors (SRs) to respond to damage/danger-associated molecular patterns (DAMPs) released by cells during injury or disease. The activation of these receptors promotes proinflammatory signaling that leads to the production of cytokines and chemokines.
Adapted from Soto I, Howell GR. The complex role of neuroinflammation in glaucoma. Cold Spring Harb Perspect Med. 2014;4(8):a017269. Published 2014 Jul 3. doi:10.1101/cshperspect.a017269

Microglial cells comprises 5-20% of the glial cells and reside in the CNS and act as the environmental stress sensors that recruit macrophages upon activation.[41] Resting (inactive) microglial cells are ramified in shape, while activated microglial cells transform into ameboid shapes. Astrocytes come in contact with neurons, blood vessels and other glial cells, providing metabolic support, modulation of synaptic activity, regulation of extracellular ion concentrations, and maintenance of the blood-ocular barrier.[34] The main function of astrocytes and microglial cells is to sense and respond to alterations and changes of the retinal microenvironment. In the case of chronic glaucoma, age-related or inflammatory disease-related stress could be recognized by glial cells through their transmembrane receptors for pathogen-associated molecular patterns (PAMPs).[42] Astrocytes and microglia cells also recognize molecules that are released by damaged cells, known as damage- (or danger-) associated molecular patterns (DAMPs). These DAMPs can also be delivered to the cell surface of damaged cells after injury.[43] Recent studies applying co-cultures of glial cells and neurons demonstrated that cytokines including interleukin-1 alpha (IL-1α) and tumor necrosis factor (TNF) released by microglia cells could activate astrocytes and induce the death of neurons including RGCs.[44]

In diseased eyes, the BRB malfunctions, and multiple types of immune cells could infiltrate into the retina. Evidence suggests the impaired BRB and induced inflammatory responses may induce pro-apoptotic cascades in RGCs.[45]

1.2.3 Inflammatory response by neurons

The specific triggers for the inflammatory pathway in glaucoma are still under study. In addition to inflammatory responses mediated by microglia cells and astrocytes that are discussed above, neurons in CNS could also directly respond to stress induced by elevated IOP.

Research of inflammatory signaling in glaucoma pathogenesis have identified that ion channels located at the surface of RGC, such as Transient receptor potential vanilloid isoform 4 (TRPV4) and pannexin-1 (Panx1), act as potential sensors and effectors of mechanical strain, ischemia and inflammatory responses.[46] These signaling pathways are associated with RGC axonal injury and cell death.

The inflammation pathway in glaucomatous eye consists of multiple levels of responses. Neuronal cells including RGCs, possibly perturbed by age-related or IOP-induced inflammatory stress, activate immune cells in CNS by releasing DAMPs and PAMPs, which could further result in the release of pro-inflammatory cytokines,[47] and contribute to neurotoxicity and loss of RGCs.[48] Alternatively, sensors on RGCs may respond to ischemia and inflammatory stress and lead to the remodeling of axons and cell death. The initiation of one form of the inflammatory response is mediated by a group of protein complexes known as the inflammasomes.

1.3 Overview of NLRP3 inflammasomes

1.3.1 Introduction of inflammasomes

Inflammasomes are a group of intracellular protein complexes that play a pivotal role in initiating a type of chronic inflammatory response.[49] Inflammasomes proteolytically cleave pro-inflammatory cytokines and lead to cell pyroptosis (a highly inflammatory form of programmed cell death[50]), which could be involved in RGC death.[51-52]

The components of the inflammasome include a sensor protein known as NOD-like receptors (NLR), the adaptor protein ASC (apoptosis-associated speck-like protein containing C-terminal caspase recruitment domain, the linker between NLRs and caspase 1), and pro-form of caspase 1 (Figure 1.4). The NLRs sense DAMPs, including bacterial/viral pathogens, pore-forming toxins, and adenosine triphosphate,[53] which are all inducers of the cell inflammatory response. The NLR family plays an important role in immune regulation. This family is composed of 22 family members, among which NLRP1, NLRP3, NLRC4 are components of the three major inflammasomes respectively. The NLR proteins contains three domains, including a N-terminal pyrin domain (PYD) that binds with the adaptor protein ASC during oligomerization, a central NACHT [NAIP (neuronal apoptosis inhibitory protein), CIITA (MHC class II transcription activator), HET-E (incompatibility locus protein from Podospora anserina) and TP1 (telomerase-associated protein)] domain functioning as ATPase that is essential for protein oligomerization during assembly, and a C-terminal leucine rich repeat domain (LRR).[54] Upon sensing certain stimuli, the NLRs or Interferon-inducible protein absent in melanoma 2 (AIM2) can oligomerize into a complex through the help of ASC, which is known as the "assembly" process. The oligomerized inflammasome will cleave the 45 kDa pro-caspase-1 into 20 kDa active caspase-1 (also known as p20), then triggering activated caspase-1 to subsequently cleave pro-forms of IL-1β and IL-18, two components of the proinflammatory IL-1 superfamily. The cleaved (mature) forms of IL-1β and IL-18 are then secreted out of the cell.

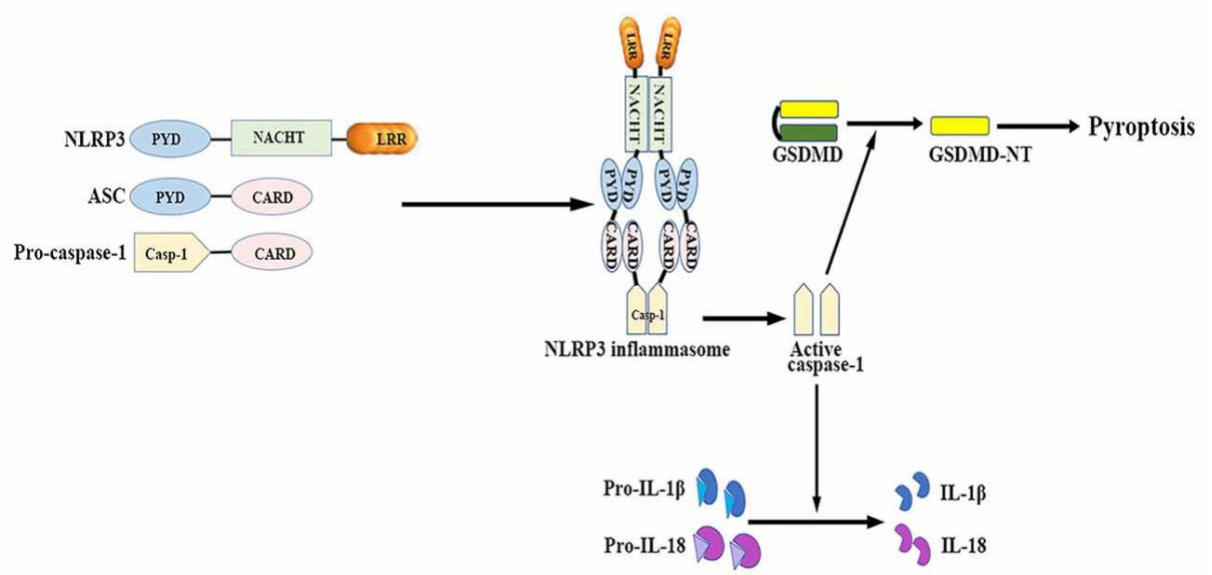

Figure 1.4 Overview of NLRP3 inflammasome structure and function. The NLRP3 inflammasome mainly consists of the sensor molecule NLRP3, the adaptor protein ASC, and the effector molecule pro-caspase-1. The assembly and activation of NLRP3 inflammasome results in caspase-1 activation. Activated caspase-1 subsequently leads to the maturation of IL-1β and IL-18, as well as cell pyroptosis. ASC: apoptosis-related speck-like protein containing a caspase recruitment domain; CARD: caspase activation and recruitment domain; GSDMD: gasdermin D; GSDMD-NT: gasdermin-N domain of GSDMD; IL: interleukin; LRR: leucine-rich repeat; NACHT (NOD): nucleotide binding and oligomerization domain; NLRP3: nucleotide-binding oligomerization domain-, leucine-rich repeat- and pyrin domain-containing 3; PYD: pyrin-only domain.
Reprinted from Song, Limin, et al. "NLRP3 inflammasome in neurological diseases, from functions to therapies." Frontiers in cellular neuroscience 11 (2017): 63.

1.3.2 NLRP3 inflammasome pathway

The overview of the inflammasome pathway is briefly described in the schematic diagram (Figure 1.4). Inflammasome formation could be triggered by a range of substances that emerge during infections, tissue damage and metabolism imbalance.[51] NLRP3 activation is unique among all kinds of inflammasomes, given its insufficient basal expression in resting cells.[55-56] Therefore a "two-signal" activation of NLRP3 inflammasomes is required, a "priming signal" to promote NLRP3 expression and an "activation" signal to trigger the inflammasome. (Figure 1.5) PAMPs usually work as a priming signal. The downstream pathway goes through the NF-kB signaling pathway, which enhances the expression of NLRP3 and pro-IL-1β. Once primed, NLRP3 can respond to an "activation" signal, which would then trigger the assembly of the NLRP3 inflammasome. For the "activation signal", several molecule candidates are proposed, including potassium ion efflux, calcium ion signaling, reactive oxygen species (ROS), mitochondrial dysfunction and lysosomal rupture.[57] The potassium ion efflux could be mediated by P2X7 receptor, a trimeric ATP-gated cation channel found dominantly in immune cells.[58]

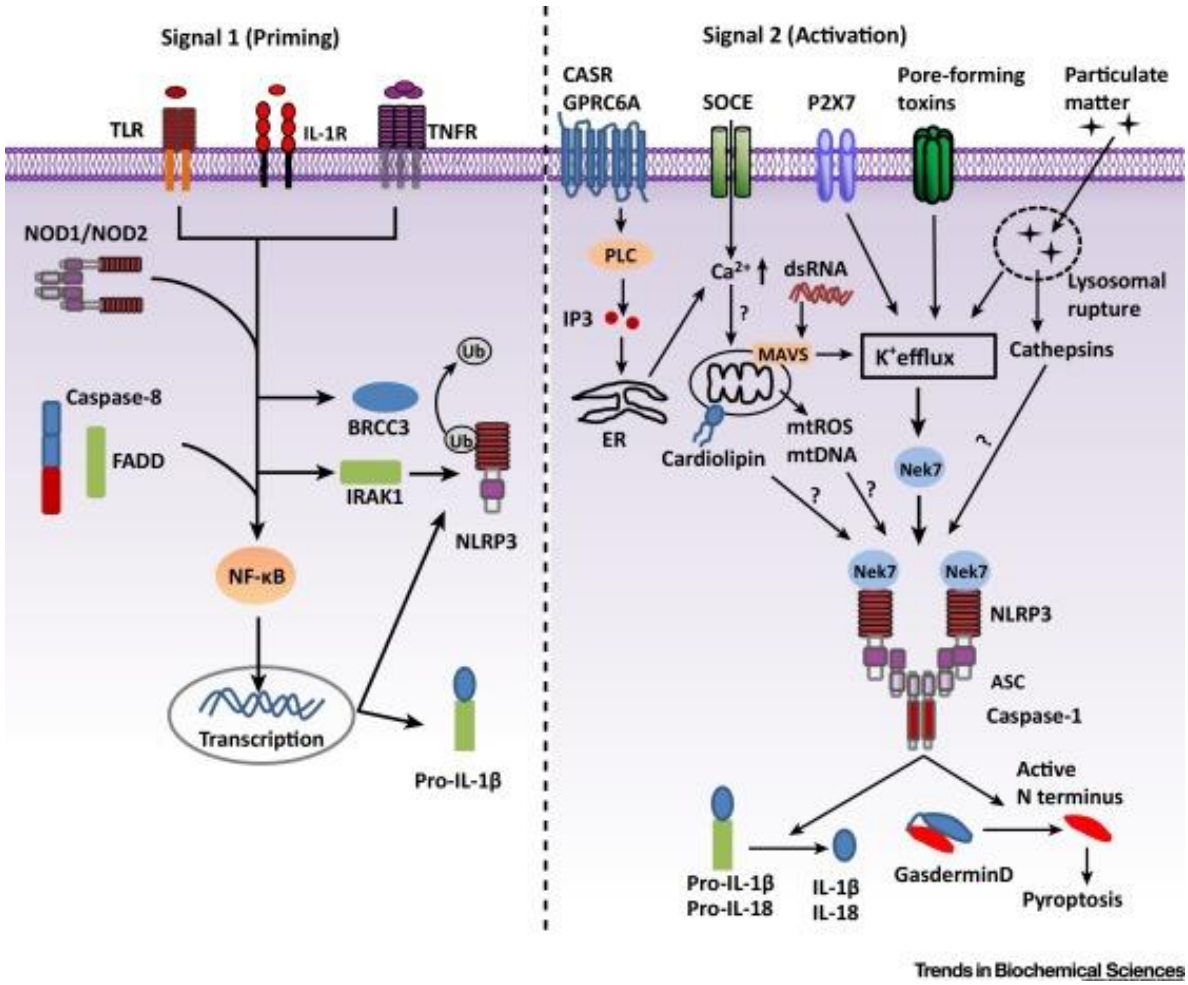

Figure 1.5 NLRP3 inflammasome priming and activation signal. Signal 1 (priming, left) is provided by microbial molecules or endogenous cytokines and leads to the upregulation of NLRP3 and pro-interleukin-1 beta (IL-1β) through the activation of the transcription factor NF-κB. Signal 2 (activation, right) is provided by a plethora of stimuli, such as ATP, pore-forming toxins, viral RNA, and particulate matter, and activates the NLRP3 inflammasome. Most NLRP3 stimuli induce K+ efflux, which is necessary and sufficient for NLRP3 activation. IL-1R: IL-1β receptor; TLR: Toll-like receptor; TNFR: tumor necrosis factor receptor.
Reprinted from He, Yuan, Hideki Hara, and Gabriel Núñez. "Mechanism and regulation of NLRP3 inflammasome activation." Trends in biochemical sciences 41.12 (2016): 1012-1021.

Once the inflammasome is activated by extracellular factors, the sensor protein oligomerizes with ASC and cleaves pro-caspase 1 into its activated form. The activated caspase-1 further cleaves IL-1β precursors into mature forms followed by their subsequent secretion. The secreted pro-inflammatory cytokines will bind to corresponding receptors and promote caspase-3 mediated cell apoptosis.

Besides pro-inflammatory cytokines that lead to cell apoptosis, recent studies have found that gasdermin D (GSDMD) is another important downstream substrate associated with NLRP3 inflammasome activation. The central role of GSDMD in inflammasome signaling is to mediate pyroptosis, a form of cell death, by pore-formation. GSDMD contains a 26 kDa N-terminal (NT) domain and a 30 kDa C-terminal (CT) domain, which are connected by a flexible linker. The CT domain functions as an auto-inhibitor molecule. Once GSDMD is cleaved by caspase-1, the NT domain is freed and subsequently oligomerizes to form pores at the cell membrane, promoting cell pyroptosis.[59-60]

Additional to the pathway discussed above, caspase-8 is an important component of inflammasome pathways as it regulates IL-1β independent of NLRP3 or NLRP1 inflammasomes.[61] Caspase-8 also promotes NLRP3 inflammasome activity as both priming and activation signal.[62]

1.3.3 NLRP3 in different models of glaucoma studies

NLRP3 is the most well-studied molecule among NLRs, due to the wide array of stimuli that link it to a variety of inflammatory diseases, including a number of neurodegenerative diseases in CNS (multiple sclerosis,[63] Alzheimer's disease, Parkinson's disease, age-related macular degeneration) and metabolic disorders including cardiovascular diseases, obesities and

type 2 diabetes.[64] Thus, the aberrant activation of the NLRP3 inflammasome has been regarded as an important initiator or promoter in a variety of human diseases,[54] including glaucoma. In acute glaucoma, the NLRP3 inflammasome is associated with microglia activation.[48, 65] In other forms of glaucoma, chronic activation of glial cells and accompanying increases in the production of proinflammatory cytokines are present.[66] Proteomic analysis of human glaucomatous postmortem eye samples has shown an increased protein expression supporting NF-kB activation in the retina, which is highly associated with NLRP3 inflammasome pathways. Further analysis demonstrates inflammasome related proteins including NLRP3 and caspase-1 were upregulated in human glaucomatous retina.[67]

Inflammasome related studies have been carried out on different acute glaucoma animal models. A recent IOP-induction acute model study reported that both the canonical pathway and non-canonical pathway of inflammasome activation play a role in saline induced hypertension in Sprague-Dawley rat eyes, where caspase-8 is an important factor in IOP-induced RGC death.[48] The suppression of caspase-8 signaling by Z-IETD-FMK (a small peptide caspase 8 inhibitor), decreased the activation of NLRP3, ASC and caspase 1, resulting in a significant decline of IL-1β. In another study using a mouse model of partial optic nerve crush (pONC) injury, activation of NLRP3-ASC inflammasome is upregulated in retinal microglial cells within 12 hours post-injury, which is highly associated with RGC death. In the pONC model, RGCs of NLRP3 knockout mice survive one week longer than control mice.[65] A recent study carried out by Pronin et al. demonstrates the activation of NLRP3 inflammasome is detected in RGCs and astrocytes exposed to the hypertension stress, which suggests that inflammasome activation induces RGC death in the retina exposed to ocular hypertension injury. The downstream products of inflammasome, including IL-1β and cleaved caspase-1, peaked 12-24 hours post ocular

hypertension injury.[37] Multiple signs of inflammasome activities also exist in DBA/2J mouse model of pigmentary glaucoma, and the details will be discussed later in section 1.4.3. Although there is significant evidence to suggest that NLRP3 inflammasome may contribute to glaucoma pathogenesis, the mechanism of how NLRP3 contributes to RGC death, and how NLRP3 inflammasomes are activated in glaucomatous eyes still remain unclear. More studies are needed in the future to address these specific questions.

1.3.4 Therapies targeting inflammasomes

Impaired inflammasome activity is involved in many human diseases and targeting the activation of the inflammasome, or its products, has become one of the potential treatment strategies for several pro-inflammatory diseases. Many reagents target the downstream pro-inflammatory cytokines IL-1β and IL-18, including recombinant IL-1ra (anakinra), neutralizing antibody against IL-1β (canakinumab), IL-18 binding protein and anti-IL-18 receptor monoclonal antibodies.[64] However, inflammasome-induced pathways independent of IL-1β and IL-18 will release DAMPs resulting in more inflammation.[68] Blocking all pro-inflammatory cytokines generated by other functioning metabolic pathways may also result in immune-compromise under certain circumstances.

Therefore, a more efficient and promising strategy for inhibition is to target the inflammasome complex itself. Several NLRP3 inflammasome specific inhibitors have been identified. The first one known as glyburide (also named glibenlamide) is a small molecule inhibitor commonly used in type 2 diabetes treatment to control blood sugar level.[69] It is also reported that glyburide has the ability to inhibit NLRP3 inflammasomes.[70] Glyburide is able to inhibit ATP- and nigericin-induced NLRP3 inflammasome activation by blocking potassium

ATP channels, an event that is downstream of P2X7 receptor and upstream of NLRP3.[70] Another inhibitor, known as ketone body β-hydroxybutyrate (BHB), functions as an alternative source of ATP and could inhibit a group of NLRP3 stimuli while not affecting other types of inflammasomes[71]. In 2017, Jiang et al. developed a compound named CY-09 that directly binds to ATP-binding motif of NLRP3 NACHT domain and inhibits NLRP3 ATPase activity, resulting in suppression of NLRP3 inflammasome activity, and ameliorating the autoinflammatory syndrome in type 2 diabetes mouse models.[72] Recently a novel NLRP3 inhibitor named JC124 was developed based on the structure of glyburide that has shown proven therapeutic values in traumatic brain injury animal model by inhibiting NLRP3 inflammasome activities.[73]

1.3.5 MCC950: A specific NLRP3 inflammasome inhibitor

MCC950 is a potent, highly selective, small-molecule inhibitor of NLRP3. It was first developed and reported by Coll et al in 2015.[74] MCC950 is one of the diarylsulfonylurea-containing compounds that was first identified as an IL-1β inhibitor. MCC950 specifically blocks canonical and noncanonical NLRP3 activation at nanomolar concentrations, without affecting AIM2, NLRC4 or NLRP1 inflammasomes. The potential mechanism of MCC950 inhibiting NLRP3 inflammasome is not clearly described by the original publication, although possibilities have been excluded, including blockade of K+ efflux. It suggests that MCC950 potentially could affect a key step of NLRP3 post-translational modifications that leads to the suppression of NLRP3 inflammasome activity.[74] A recent study suggests that MCC950 may bind to NACHT domain of NLRP3 that inhibits the inflammasome assembly upon activation.[75]

MCC950 has been well studied and used in many disease models that are influenced by NLRP3 inflammasome activities, such as type 2 diabetes, traumatic brain injuries and many

autoimmune diseases. Various methods of MCC950 administration in animal models is also involved, including oral administration,[76-77] intravenous injections[78] and intraperitoneal injection,[79-81] the duration of which varies from 1 week to 3 months. In this study, MCC950 is used to assess its ability to suppress NLRP3 inflammasome activity. The methods and results are described in section 2.2 and section 3.8-3.10.

1.4 Background of DBA/2J mouse model of glaucoma

1.4.1 Genetics of the DBA/2J mouse strain

The DBA/2J is a commonly used inbred mouse strain. DBA/2J strain is developed from DBA strain (first inbred strain bred by Clarence Little in 1909) by Jackson Laboratory. It is firstly discovered as ocular abnormalities associated with iris atrophy by John et al. in 1998.[82] DBA/2J was then identified as a mouse model for ocular hypertension. It is a valuable model because it mimics human glaucoma, including the age-related variable onset of IOP elevation, progressive optic nerve axon damage and RGC loss.[83] It has been widely used in glaucoma studies.[84] DBA/2J mice develop a form of pigmentary glaucoma involving iris pigment dispersion (IPD) and iris stromal atrophy (ISA). The IPD in DBA/2J leads to blockage of trabecular meshwork and causes IOP elevation, which is similar to POAG. However, the DBA/2J iris forms a tight angle with cornea due to iris degeneration, which appears to be a closed angle component to the glaucoma unlike humans.[84]

DBA/2J contains many gene mutations, among which two of the genes are responsible for the anterior chamber phenotypes: *Trp1*^{isa} and *Gpnmb*^{R150X}. *Trp1*^{isa} is an abbreviation for tyrosinase related protein 1, encoding a component of a melanosome membrane protein complex involved in pigment production, it is located at chromosome 4, which is responsible for ISA. The

study suggests that homozygosity of *Trp1b* may possibly cause abnormality of melanosome membrane protein structure that result in leakage of intermediates of pigment production, which could lead to subsequent cell death and ISA[85]. *Gpnmb*^{R150X} is an abbreviation for glycoprotein nonmetastatic melanoma protein B, this gene is located on chromosome 6, and linked to IPD, which is characterized by deterioration of the posterior iris pigments. Sequencing of *Gpnmb*^{R150X} detected a premature stop codon within the fourth of eleven exons, the truncated protein lacking a C-terminal dileucine melanosome sorting motif result in disruption and leakage of pigment production[86]. This phenotype is exclusive in homozygote DBA/2J mice while in heterozygotes IPD (and elevated IOP) do not occur[87]. The pigment dispersion syndrome caused by *Gpnmb*^{R150X} mutation has similarities to human PDS, including a pattern of radial iris depigmentation, which is considered as a hallmark of human PDS. Therefore, DBA/2J mice provide a valuable resource for defining factors that may contribute to human pigmentary glaucoma (a form of secondary glaucoma).[88-89]

1.4.2 Phenotype and related studies of DBA/2J

It has been demonstrated that the DBA/2J strain spontaneously generates age-related IOP elevation caused by the mild to severe ISA and IPD at the anterior segment.[82] Female DBA/2J mice at 6 months of age start to show a significant increase in IOP (compared to males). Between 6-9 months of age, the IOP further increases in both males and females.[90] Accompanying the IOP elevation, RGC loss is observed. The density of RGCs is dramatically lowered in 9-month DBA/2J mice, with corresponding optic nerve damage.[90-91]

Elevated IOP is not the only factor that causes RGC death. Signs of inflammatory response in the DBA/2J mouse eye has been evident, including upregulated TLRs and TLR

adaptor protein MyD88 in the ONH.[34] These signs of inflammatory response are possibly associated with RGC death. Microglia activation presents in DBA/2J retina, pre-laminar optic nerve and optic nerve head.[92] Cytokine signaling dysregulation in the retina and optic nerve head of DBA/2J mice is also evident. Significant elevations in retinal pro-inflammatory cytokines were observed in the retina and optic nerve head of DBA/2J, including IL-1β and TNF-α,[93] suggesting the involvement of an inflammatory pathway in the progression of RGC death.

1.4.3 Potential of inflammasome activity in DBA/2J

Studies using a database constructed from Glaucoma Discovery Platform (GDP) from the Jackson Laboratory have demonstrated that in the DBA/2J mice, 11 of 13 TLRs are up-regulated in the ONH; The TLRs adaptor protein MyD88, which is the upstream inducer of NLRP3 inflammasome, is also up-regulated in the retinas and the ONH of DBA/2J mice. Genes encoding proteins associated with inflammasome pathway, including *casp1* (encodes caspase-1) and *il1b* (encodes IL-1β) have been found to be upregulated in DBA/2J retina.[83] These findings suggest that inflammasome activity exists in this mouse model of glaucoma.

1.4.4 Other animal models in glaucoma study

Animal models of different species are used in glaucoma studies, including monkeys,[94] rabbits, and smaller animals such as rodents.[95] A wide variety of animal models are developed and used to study different types of glaucoma. These models can be generally divided into three categories according to glaucoma types: animal models for POAG, PACG and other types of glaucoma.

For POAG studies, both spontaneous monkey models (rhesus monkeys) and experimental monkey models (induced ocular hypertension by photocoagulation) were used. [96] Transgenic mouse models are also used to study POAG, including a mouse strain expressing the Tyr423His myocilin (one of the causative genes in human POAG) point mutation, and another transgenic mouse strain with a targeted mutation in the gene for the α1 subunit of collagen type I.[97-98] Experimental rat models (induced hypertension) was also used in POAG studies. [99] For PACG studies, Vav2/Vav3-deficient mice were described and found to have elevated IOP and choric angle closure.[100] Besides rodents, dog models and turkey models are also used in PACG studies.[84] Each animal model has its strengths and limitations. Monkeys share similar phylogeny and high homology to humans, which makes it an ideal model for studying. However, monkeys are expensive and requires experienced teams/facilities to handle. Transgenic mice are relatively cost-effective, but the small size of globe makes it hard to perform tissue separation/purification in study.

DBA/2J mice have symptoms similar to human pigmentary glaucoma, as described in previous sections. This mouse strain develops a progressive IOP elevation with age, which is similar to human glaucoma.[86] Although DBA/2J mouse strain has been well-characterized in chronic glaucoma studies, it has some limitations as well. The disease progression is not uniform in two eyes of the same animal or mice in the same age, therefore larger sample size is normally used to overcome this issue. More details will be discussed in the discussion section.

1.5 Study objectives, hypothesis, rationales and significance

The overall objective of this study is to determine whether the activation of inflammasome contributes to the RGC death in the DBA/2J mouse model of glaucoma, a neuroinflammatory disease. The aims of the study are as follow:

Aim 1: To determine whether there are changes in activity of the NLRP3 inflammasome in DBA/2J retina during aging and IOP elevation.

Sub Aim 1: To determine whether NLRP3 expression is increased in DBA/2J at 9 months compared to 3 months of age.

Sub Aim 2: To determine whether caspase-1 and GSDMD expression level is increased in DBA/2J at 9 months compared to 3 months of age.

Sub Aim 3: To determine whether NLRP3 inflammasome activity is associated with microglial cell activities.

Aim 2: To determine whether the NLRP3 inflammasome activity is associated with elevated IOP in DBA/2J mouse model.

Sub Aim 1: To determine whether NLRP3 expression level is correlated with IOP elevation.

Sub Aim 2: To determine whether caspase-1 expression level is correlated with IOP elevation.

Aim 3: To determine whether the NLRP3 inflammasome contributes to RGC death in DBA/2J mouse model.

Sub Aim 1: To determine whether there is RGC loss in 9-month compared to 3 months of age in DBA/2J.

Sub Aim 2: To determine whether inhibition of NLRP3 inflammasome affects RGC loss.

The overall hypothesis of this study is that the elevation of IOP in aged DBA/2J eyes leads to the activation of the inflammasome, and thereby contributes to RGC death in the DBA/2J mouse model of glaucoma.

The overall rationale of this study is that glaucoma is a neurodegenerative disease, and early neuroinflammatory responses by microglia, and other blood-derived immune cells are observed in the RGC layer, suggesting a primary role of inflammation in chronic glaucoma.[34, 93] Evidence suggests that inflammasome activation and subsequent pro-inflammatory cytokine release contribute to RGC death in acute glaucoma.[48] However, it is not known whether inflammasomes also contribute to RGC death in chronic glaucoma. Therefore, we studied inflammasome activities in DBA/2J mouse model of chronic glaucoma to assess this question.

DBA/2J mouse model spontaneously generates elevated IOP, which better mimics chronic glaucoma in humans. As the DBA/2J is an inherited mouse model, it does not require surgical procedures to induce elevated IOP, therefore eliminates surgically induced physical damage which could also lead to inflammasome activation. Furthermore, there is existing evidence that dysregulation of cytokine signaling in the RGC layer of DBA/2J mice is present,[93] which further supports the possibility of inflammasome activities in DBA/2J retina.

The overall significance of this study is that it may shed light on whether inhibition of inflammasome activity by a small molecule drug may be a potential treatment strategy to rescue RGCs from cell death in human glaucoma.

Chapter 2: Materials and Methods

2.1 DBA/2J Animal Husbandry

Female DBA/2J mice were purchased from Jackson Laboratory (000671-DBA/2J) at 3-7 months of age and housed at Jack Bell Research Centre, in accordance with the University of British Columbia Animal Care Committee guideline under ACC protocol number A17-0229. All mice were quarantined for 7 days prior to housing in normal animal caging area. A total of 35 DBA/2J mice were used to assess intraocular pressure changes and inflammasome activity. A total of 8 C57BL/6J mice were studied as controls for age-related increases in inflammasome activation. As C57BL/6J mice do not exhibit age-related IOP elevation,[101] these animals were used to assess age-related increases in inflammasome proteins.[91] For baseline data on DBA/2J, 7 mice were sacrificed at 3 months of age; 7 mice were sacrificed at 9 months of age; 10 mice were treated and sacrificed in pilot drug treatment study; 8 mice were treated and sacrificed in final treatment group, and 3 mice were sacrificed at the same age and time as the treatment control (Table 2.1).

Group	ID	DOB	Date of sacrifice	Age at sacrifice	Eye	
					OS	OD
3m Baseline	**Y-1***	May-1-2018	Jul-27-2018	2m27d	FFPE	Frozen/protein lysate extracted
	Y-2*		Jul-27-2018	2m27d	FFPE	Frozen/protein lysate extracted
	Y-11*	Sep-11-2018	Dec-11-2018	3m	FFPE	Frozen/protein lysate extracted
	Y-12*				FFPE	Frozen/protein lysate extracted
	Y-13				FFPE	Whole mount processed
	Y-14*				Frozen/protein lysate extracted	Whole mount processed
	Y-15*				Frozen/protein lysate extracted	Whole mount processed
9m Baseline	**Y-6***	May-1-2018	Feb-01-2019	9m	FFPE	Frozen/protein lysate extracted
	Y-7*			9m	FFPE	Frozen/protein lysate extracted
	Y-8			9m	FFPE	Whole mount processed
	Y-9*			9m	Whole mount processed	Frozen/protein lysate extracted
	Y-10*			9m	Whole mount processed	Frozen/protein lysate extracted
	O-1*	Oct-24-2017	Jul-27-2018	9m3d	FFPE	Frozen/protein lysate extracted
	O-2*			9m3d	FFPE	Frozen/protein lysate extracted
MCC950 test	Y-3	May-1-2018	Sep-13-2018	4m13d	FFPE	FFPE
	O-6	Nov-14-2017		9m30d	FFPE	Formalin fixed
MCC950 test-2	**Y-4**	May-1-2018	Oct-5-2018	5m4d	Frozen/MCC950 analysis	Frozen/MCC950 analysis
	Y-5			5m4d	Frozen/MCC950 analysis	Frozen/MCC950 analysis
	O-7	Nov-21-2017		10m14d	Frozen/MCC950 analysis	Frozen/MCC950 analysis
	O-8			10m14d	Frozen/MCC950 analysis	Frozen/MCC950 analysis

Group	ID	DOB	Date of sacrifice	Age at sacrifice	Eyes	
					OS	OD
MCC950 food trial	O-9	Nov-21-2017	Dec-14-2018	12m23d	Frozen/MCC950 analysis	Frozen/MCC950 analysis
	O-10			12m23d	Frozen/MCC950 analysis	Frozen/MCC950 analysis
Food trial control	O-11	Apr-03-2018	Dead on Mar-15	11m12d	Formalin fixed	Formalin fixed
	O-12		Apr-03-2019	12m	Frozen/protein lysate extracted	Frozen/protein lysate extracted
Treatment group	T-1	Jul-17-2018	Apr-23-2019	9m6d	Whole mount processed	Frozen/protein lysate extracted
	T-2				FFPE	Frozen/protein lysate extracted
	T-3				FFPE	Frozen/protein lysate extracted
	T-4	Jul-31-2018		8m22d	Whole mount processed	Frozen/protein lysate extracted
	T-5				Frozen/protein lysate extracted	Whole mount processed
	T-6				FFPE	Frozen/protein lysate extracted
	T-8	Jul-24-2018		8m29d	FFPE	Whole mount processed
	T-9	Jul-31-2018		8m22d	Whole mount in fix	Frozen/protein lysate extracted
Treatment control (pellet only)	Ctrl-1	Jul-10-2018	Apr-23-2019	9m13d	Whole mount processed	Whole mount in fix
	Ctrl-2				Whole mount	Frozen/protein lysate extracted
	Ctrl-3				Whole mount	Frozen/protein lysate extracted

Table 2.1 Grouping and animal ID of DBA/2J used in this study. M: month; d: days; FFPE: formalin fixed paraffin embedded; DOB: date of birth; animal ID in bold font: IOP measure used in Figure 3.1; animal ID with asterisk: IOP measure used in Figure 3.5.

2.2 MCC950 administration

A total of 9 DBA/2J mice (7 months of age) were fed daily at 7:30 am for 8 weeks with 1.5 g Transgenic Dough Diet™ (BioServ®) well mixed with 20 mg/kg MCC950 (Selleck Chemicals). These animals were sacrificed after 8 weeks of drug treatment (at 9 months of age). Mice of the treatment group were caged by two, with a divider to separate two mice in the same cage to ensure that each mouse received the appropriate levels of drug. Each food pellet was specifically made for each mouse. A certain volume of MCC950 (20 mg/ml) was mixed with dough diet (1.5 g) according to the corresponding mouse bodyweight measured once a week. The food pellets were mixed two days prior to use and were stored at 4 deg C. Food pellets without drug were given to control mice. Food pellets (with/without drug for treatment/control group) were distributed to the cage at 7:00 am in the morning. When the pellets were completely consumed, the regular mouse chow would be placed in the cage as per routine maintenance and care. After 8 weeks of drug treatment, blood samples were taken by tail vein following UBC Animal Care Guidelines (SOP: ACC 2014 Tech12). Next, animals were euthanized by carbon dioxide euthanasia, one eye and both kidneys were immediately dissected and frozen in dry ice. The other eye was fixed in 10% formalin. Four C57BL/6J mice were sacrificed as 3- and 9-month old age-matched controls.

2.3 Intraocular pressure (IOP) measurement

IOP measurements were performed every two weeks. DBA/2J mice were anesthetized by isoflurane inhalation, then transferred to a platform under gentle restraint. After the mice were anesthetized, 3 serial measurements of IOP (mmHg) for each eye were measured by Tonolab© tonometer. The final IOP value (mmHg) is the average of the three measurements. An integrated

data from both left and right eyes of individual DBA/2J were plotted in the diagram shown in result section 3.1 and 3.6.

2.4 Serum/tissue analysis of MCC950 level

Mouse blood samples were centrifuged at 4 deg C, 12 G for 20 minutes to separate the serum and frozen until analysis. Serum samples from *in vivo* studies were thawed and 8µl transferred to individual Eppendorf tubes followed by addition of internal standard (IS, 2 µl of 2.4 µg/ml glipizide (Glip)) and brief vortexing. 22 µl of methanol/acetonitrile (50/50) was then added, samples again vortexed, and precipitated protein sedimented by centrifugation (5 min, 20000 g). Clarified supernatant was transferred to LC vials. Standards were prepared in a similar fashion with MCC950/IS spiked blank mouse serum; parallel standards made up in solvent only were used to characterize any matrix effects. Tissue samples (50-200 mg) were weighed, two volumes water added, and samples homogenized using a Precellys tissue homogenizer (Bertin Technologies) with 2 x 45 second cycles at 5500 rpm. Extraction was similar to serum but using 16 µl homogenate, 4 µl IS and 44 µl solvent; spiked serum samples were used for calibration.

An acuity Ultra-Performance Liquid Chromatography (UPLC) coupled with a Quattro Premier (Waters) was used for analysis. Separations were carried out with a 100mm BEH C18, 1.7 µ column (Waters) and an acetonitrile (ACN) gradient (0-0.2 min, 40%; 0.2-2.75 min, 40-85%; 2.75-3 min, 85-98%; 3-6, 98%; 6-6.1 min, 98-40%; 0.3 ml/min, 8 min total run length; 0.1% formic acid present throughout). MS data was collected in ES negative slightly below unit resolution with the following instrument parameters: capillary, 3 kV; extractor and RF lens, 6 V and 0.1 V; source and desolvation temperatures, 120 deg C and 300 deg C; desolvation and cone (N_2) flow, 1000 L/hr and 50 L/hr; collision gas (Ar) flow, 0.15 ml/min ($8e^{-3}$ m bar). Compounds

were detected by multiple reaction monitoring (MRM) with m/z 403.3>204.3 and 403.3>80.2 for MCC950 and m/z 444.2>170 and 444.2>319.2 for Glip (37V/22V, 37V/37V and 35V/37V 35V/22V cone/collision volt combinations respectively) with 0.1 sec dwell each. Retention times for MCC950 and Glip were 2.6 min and 2.05 min respectively.

Data was processed using Quanlynx (Waters) using AUC ratios of MCC950/Glip for calibration and quantification and exported to Excel for further analysis. Calibration standards ranged from 1.5 to 1500 ng/ml (6 points, extract levels). A linear fit was used resulting in R_2 >0.99, and deviation from nominal < 15% above 1.5 ng/ml. Some matrix suppression (<25%) was observed with Glip but very little with MCC950 in both serum and tissue extracts. These procedures were undertaken in collaboration with Mr. Hans Adomat, Vancouver Prostate Cancer Centre.

2.5 Tissue processing for immunohistochemistry (IHC) and immunofluorescence (IF)

All procedures were performed according to previous methods carried out in Dr. Matsubara's lab.[102] Mouse eyes were fixed in formalin for 48 hours before paraffin embedding. Formalin fixed, paraffin embedded (FFPE) eyes were sectioned by microtome at the thickness of 6 μm. After sectioning, tissue sections on glass slides were stored at room temperature and deparaffinized before IHC or IF processing. For deparaffinization, the tissue sections on glass slides were placed in two sequential containers of xylene for 5 minutes each, then placed in three sequential containers of 100% ethanol for 2 minutes each, then placed in descending concentrations of ethanol (95%, 70%, 50%) for 2 minutes each, and rehydrated in distilled water for 5 minutes.

For whole-mount preparation, the mouse eyes were previously fixed in 10% formalin overnight. On the next day, the eyes were cut around the circumference of the limbus under a dissecting microscope. After finishing the cut, the cornea, iris, lens and sclera were carefully removed by forceps. The retinas were gently dissected from the eyecup and stored free-floating in formalin at 4 deg C.

Both FFPE sections and whole-mount retinas were then washed in PBS (pH 7.2-7.4) three times at room temperature (RT). For antigen retrieval, FFPE sections were incubated in proteinase K diluted 1:200 in Tris-EDTA buffer (pH 9.0) for 10 minutes at RT. Alternatively, tissue sections/whole-mounts were heated in citrate buffer (pH 6.0) for 10-15 minutes at 95 deg C in microwave at power level of 800. Then sections/whole-mount retinas were washed three times in PBS followed by endogenous peroxidase activity blocking, incubated in 3% H2O2 in distilled water. Sections were blocked in 3% of normal goat serum (Vector Laboratories) in PBS with 0.3% TX-100. The following primary antibodies were diluted in 3% normal goat serum, incubated for 1 hour at room temperature and overnight at 4 deg C: anti-NLRP3 (1:100, AG-20B-0014-C100 Adipogen), RBPMS (1:200, sc-293285 Santa Cruz Biotechnology), IBA-1 (1:1000, 019-19741 Wako Chemicals). Sections/whole-mount retinas were washed three times in PBS, incubated in the following secondary antibody for 45 minutes in RT: biotinylated goat anti mouse secondary antibody (1:200, BA-9200 Vector Laboratories), biotinylated goat anti rabbit secondary antibody (1:200, BA-1000 Vector Laboratories), goat anti mouse Alexa 546 (1:200). For IHC sections, staining was detected by ABC HRP kit (Vector Laboratories) and counterstained with hematoxylin. For IF, sections and whole-mount retinas were counterstained with DAPI (1:500) for 15 minutes in at RT and washed well in PBS four times with 15 minutes

each. Slides were mounted by aqueous mount (Glycerol: PBS=1:1) and cover-slipped with coverslips of 0.1mm or 0.15mm thickness. See Table 2.2 for all antibodies used.

Antibodies/reagents	**Company/Lot #**	**Application**	**Dilution rate**
normal goat serum	Vector Laboratories S-1000	IHC/IF	1:20
Anti-NLRP3	Adipogen AG-20B-0014-C100	IHC	1:100
Anti-RBPMS	Santa Cruz sc-293285	IF	1:200
Anti-IBA-1	Wako Chemicals 019-19741	IHC	1:1000
biotinylated goat anti mouse secondary antibody	Vector Laboratories BA-9200	IHC	1:200
goat anti mouse Alexa 546	Thermo Fisher Scientific A-21133	IF	1:200
ABC HRP kit	Vector Laboratories PK-4000	IHC	
DAPI	Vector Laboratories H-1200	IHC/IF	1:500
Anti-Caspase-1	R&D systems 661228	Western blot	1:1000
Anti-GSDMDC1 (A-7)	Santa Cruz sc-393656	Western blot	1:100
Anti-IL-18	Abcam ab71495	Western blot	1:1000
Anti-GAPDH	Abcam	Western blot	1:20000

Table 2.2 List of antibodies and reagents used in experiments. IHC: Immunohistochemistry; IF: Immunofluorescent.

2.6 Z-stack imaging of IF and staining analysis

Z-stack images of immunofluorescent-stained whole-mount retinas were taken by confocal microscope (Zeiss LSM Laser 800 microscope). The whole-mount retinas were dissected into two halves before immunostaining. One of the two halves from each eye was processed and imaged under 20X magnification. The image was segmented into three concentric circles with equal intervals to each other, and the circles are centred at the ONH (Figure 3.9). The inner-most circle represents the central area of the retina, the middle circle represents the mid-peripheral area and the outer-most retina represents the far-peripheral area of the retina.

Four areas evenly distributed within each region were selected for z-stack imaging. Z-stack images were taken under fixed intervals (650 nm) and 8-10 optical slices were contained per z-stack image with a total thickness of 5.2 μm-6 μm. Image sequence was exported by ZEN 2.6 and compressed by Image J.

2.7 IHC brightfield analysis

The images of IHC stained cross sections were taken under 60X Nikon eclipse 80i microscope. The retinas were divided into three areas including central area, mid-peripheral area and far-peripheral area (Figure 2.1). A fixed-size sample box (1000 pixels by 150 pixels, centered over RGC layer and 600 pixels by 600 pixels centered over ciliary body) was applied for each image during analysis. The colors representing a positive staining are manually selected using Photoshop. The non-specific background label within the sample box is eliminated by deselecting colors from negative control images, thereby generating a color range for quantification of the positive immunolabeling. After setting up, the number of pixels in the sample box that displayed colors within the color range was calculated by using the histogram tool in Photoshop.

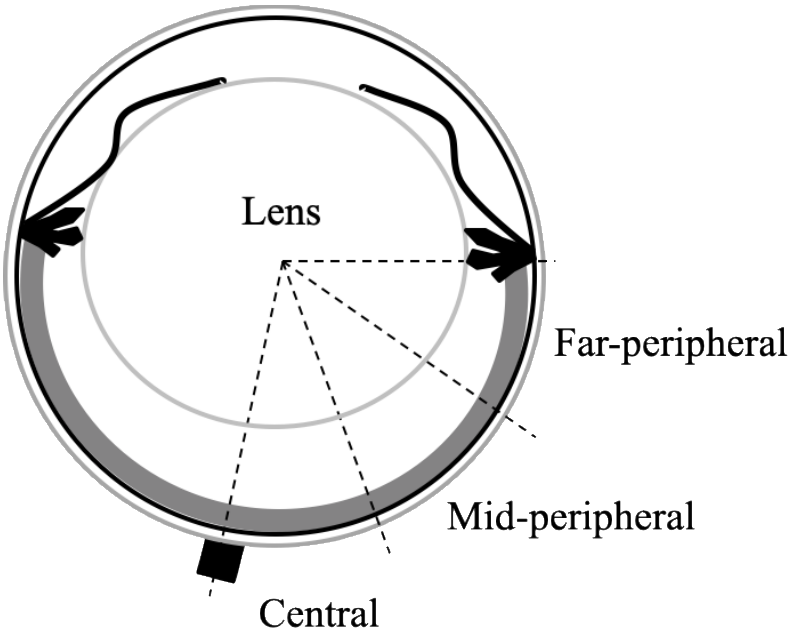

Figure 2.1. Schematic of areas for immunolabeling analysis. DBA/2J retinas were divided into three areas, including central area, mid-peripheral area and peripheral area.

2.8 Lysate preparation and Western Blot analysis

DBA/2J and C57BL/6J eyes taken immediately after euthanasia were kept frozen at -80 deg C. For protein lysate preparation, eyes were dissected on ice, muscle attachments and lens were carefully removed and discarded. Remaining tissues (including retina and uvea) were homogenized by Fisherbrand handheld homogenizer in radioimmunoprecipitation assay (RIPA) buffer with proteinase inhibitor and subsequently centrifuged at 4 deg C, 14.8 G for 30 min to separate the protein. Supernatant were aliquoted and stored at -80 deg C. The protein concentration of each sample was measured by bicinchoninic acid (BCA) assay. For Western blot analysis, 10-50 μg protein lysate from each sample was loaded onto 10% resolving gel and subsequently transferred to a polyvinylidene difluoride (PVDF) membrane, blocked in 5% milk in TBS for 1 hour in room temperature. The membrane is subsequently incubated in the

following antibody diluted in 5% milk-TBS overnight: caspase-1 (1:1000), GSDMD (1:100, Santa Cruz Biotechnology), IL-18 (1:1000, Abcam), GAPDH (1:20000, Abcam). Secondary anti-mouse or anti-rabbit HRP antibody was used, respectively. The membranes were developed on x-ray film in darkroom for 2-10 minutes. Results were analyzed by Image J Gel plotting.

2.9 Statistical analysis

Multiple ways of significance test were performed for different data sets of this study. All statistical tests were performed by Graph Pad software.

IOP measurements: one-way/two-way ANOVA test followed by Tukey's *post hoc* analysis was performed to compare age-related changes of IOP (Figure 3.1 and Figure 3.9 respectively).

NLRP3 IHC experiments: Mann-Whitney tests were performed to compare between two age groups (Figure 3.3 C and Figure 3.11 C). Two-way ANOVA test were performed to compare between two age groups and central/peripheral areas (Figure 3.2 G and Figure 3.10 E). Bonferroni *post hoc* test was used instead of Tukey's test due to the relatively small sample size.

IBA-1 IHC experiments: the number of microglial cells was manually scored; non-parametric Mann-Whitney was performed for a significance test (Figure 3.7 and Figure 3.14).

Western blot analysis: the intensities of protein bands were normalized to fold-changes. Student t-tests were performed for significance tests (Figure 3.4 and Figure 3.12). Outliers of data were detected and removed by Grubbs' test with alpha=0.05.

RGC measurements: Using Z-stack images, RGCs were counted manually, by individuals masked to the identity of the datasets. The results were analyzed by two-way ANOVA followed by Tukey's *post hoc* test (Figure 3.13).

Chapter 3: Results

To better understand the role of NLRP3 inflammasome activity in the DBA/2J mouse model, we divided the study into two major parts: 1) the baseline study of DBA/2J to examine whether NLRP3 inflammasome activity changes with IOP or aging; 2) the drug treatment study targeting NLRP3 inflammasome with MCC950 to determine whether NLRP3 inflammasome activity contributes to RGC loss in DBA/2J.

3.1 Confirmed IOP is elevated in DBA/2J during aging

In our cohort of mice, we observed a similar change in IOP during aging as expected.[82] The mean IOP of 3-month old DBA/2J was 11.40±0.57 mmHg, and at 7 months of age the mean IOP was unchanged at 11.49±1.073 mmHg. At 9 months of age, the mean of IOP increased to 15.09±1.028 mmHg (Figure 3.1). A one-way ANOVA was conducted to compare the effect of age on IOP in 3-month, 5-month, 7-month and 9-month conditions. There was a significant effect of age on IOP at $p<0.05$ level for the four conditions [$F(3,46) = 5.952$, $p=0.0016$]. Tukey's *post hoc* comparisons indicate that there were significant differences between 9-month group and all other younger groups. To note, the standard error of the mean of IOP in 9-month old DBA/2J was also increased suggesting inter-animal variability.

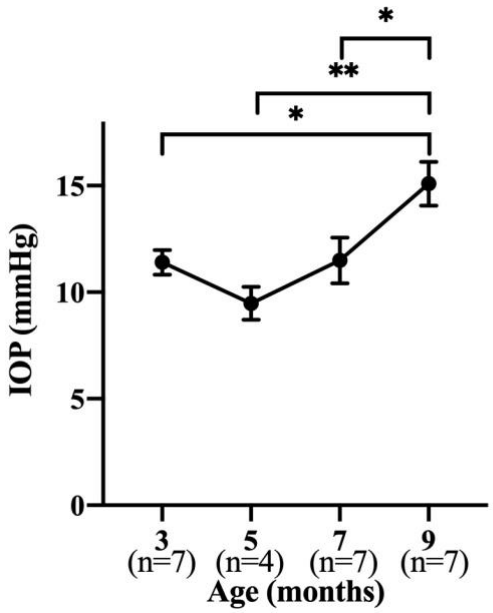

Figure 3.1 Mean intraocular pressure (IOP) measurements of DBA/2J. The intraocular pressure was tested every two months from 3 to 9 months of age. IOP was measured by a Tonolab© tonometer. Measurements were taken at the same time of the day throughout the study to avoid diurnal changes in IOP. Data were collected from both eyes of each animal. (MEAN±SEM, One-way ANOVA indicate a significant effect of age on IOP [$F(3,46)=5.952$, $p=0.0016$], followed by Tukey's *post hoc* test, n=7 for 3, 7and 9-month DBA/2J, n=4 for 5-month DBA/2J; 2 eyes/mouse, ***$p<0.001$).

3.2 Age-dependent increase of NLRP3 expression on DBA/2J retina and ciliary body

DBA/2J mice were divided into two groups based on their age: a 3-month DBA/2J group (younger group) and a 9-month DBA/2J group (older group). NLRP3 immunohistochemistry (IHC) on DBA/2J retina cross sections were performed to examine the expression pattern of NLRP3. The immunolabeling pattern suggests that NLRP3 is mainly expressed within the RGCs, with less expression detected at the inner nuclear layer (INL) (Figure 3.2, A-D). Both central and peripheral regions of the 9-month DBA/2J retina demonstrate a strong positive labeling of NLRP3, while the NLRP3 immunoreactivity in 3-month DBA/2J is at a significantly lower level. A two-way ANOVA was conducted that examined the effect of age and retinal regions on NLRP3 immunolabelling. There was a statistically significant effect of age on NLRP3 immunolabelling [$F(1,28) = 21.51$, $p < 0.001$]. Bonferroni *post hoc* test showed that 9-month DBA/2J NLRP3 immunolabelling was significantly higher than 3-month DBA/2J in both central and mid-peripheral regions of retina. However, within the same age group, there is no significant difference between central and peripheral areas (Figure 3.2, G). This suggests that central and peripheral retina do not vary in levels of NLRP3 expression within a given group.

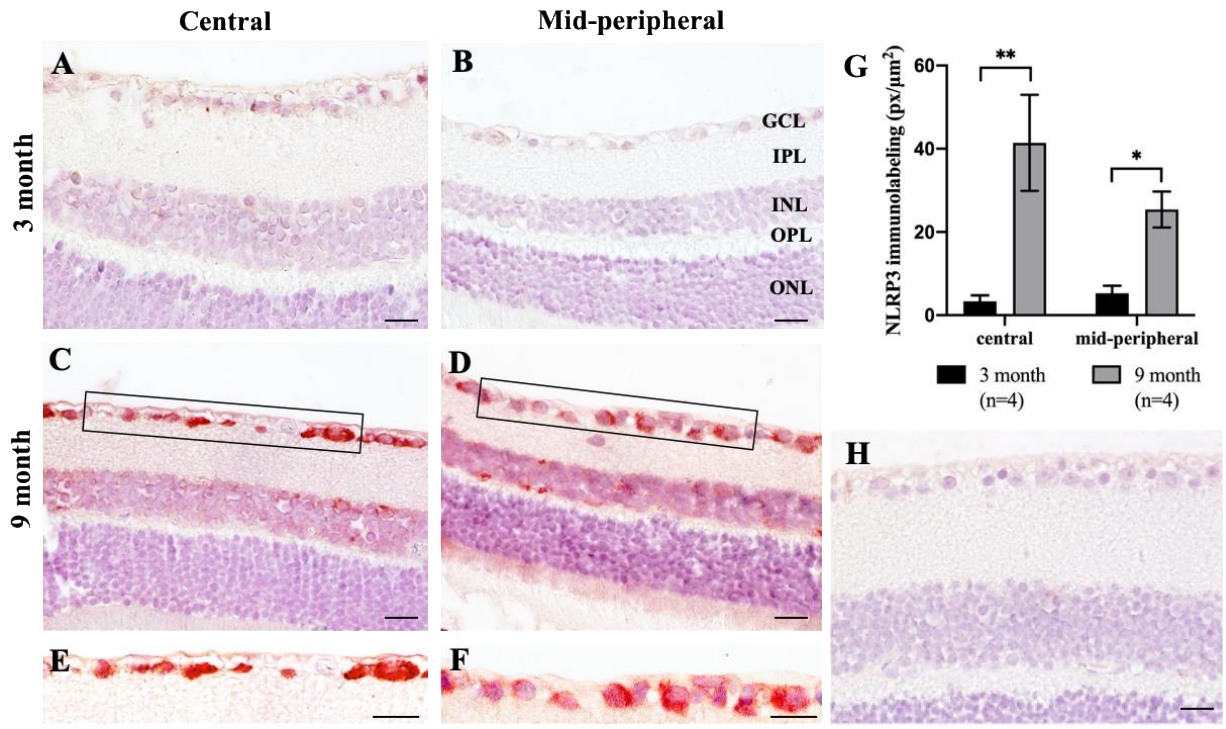

Figure 3.2 NLRP3 immunohistochemistry (IHC) results in DBA/2J retina. NLRP3 (Cryo-2) IHC staining on 3-month and 9-month-old DBA/2J mouse retinal ganglion cells (A-D, red=NLRP3). Enlargements of the rectangle in C and D (E, F); corresponding total NLRP3 staining is quantified by pixel numbers of certain threshold (manually selected in photoshop, background eliminated by deselecting colors from negative control image) inside a fixed-size sample box (indicated as the rectangle in C-D) and negative control (IHC staining on DBA/2J cross-sections without primary antibody) (H). Two-way ANOVA indicated a statistically significant effect of age on NLRP3 labelling [$F(1,28) = 21.51$, $p<0.001$], followed by Bonferroni's *post hoc* test (G, Mean ± SEM, n=4,*$p<0.05$, 2 data points per retinal area per mouse, **$p<0.01$). GCL: ganglion cell layer; IPL: inner plexiform layer; INL: inner nuclear layer; OPL: outer plexiform layer; ONL: outer nuclear layer; Scale bar=10 μm.

NLRP3 expression is also detected in the epithelial cells of the ciliary body (Figure 3.3 A, B). By analyzing with t-test, this result demonstrates the NLRP3 labeling density of 9-month DBA/2J is significantly greater than observed in 3-month DBA/2J (Figure 3.3 C). These results indicate that NLRP3 inflammasome expression increases in the older DBA/2J mice. However,

this does not indicate that inflammasome activation increases in older DBA/2J mice, as IHC expression can only determine total NLRP3 protein levels, but not activity.

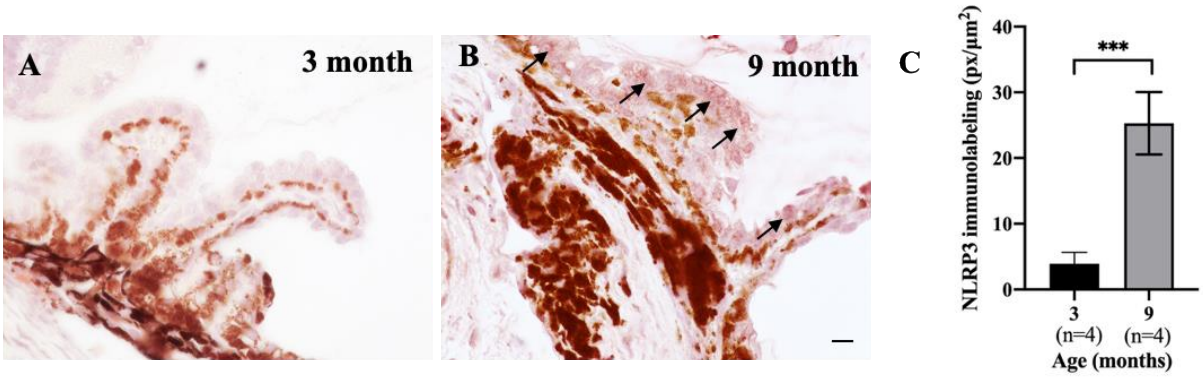

Figure 3.3 NLRP3 immunohistochemistry (IHC) results in DBA/2J ciliary body. NLRP3 (Cryo-2) IHC staining on 3-month and 9-month-old DBA/2J ciliary body (A-B, asterisks); corresponding total NLRP3 staining is quantified by pixel numbers of certain threshold (manually selected in photoshop, background eliminated by deselecting colors from negative control image) inside a fixed-size sample box. Mann-Whitney test was used for statistical analysis (C, Mean ± SEM, n=4, 1 eye/mouse, *p<0.05, ***p<0.001). Scale bar=10 μm.

3.3 Age-dependent increase of inflammasome activation by caspase-1 cleavage and GSDMD expression in DBA/2J eyes

We examined the protein expression level of caspase-1 and inflammasome downstream proteins GSDMD by western blot of DBA/2J whole-eye lysate. Both the pro-form and the active forms of caspase-1 and GSDMD are detected by their respective antibodies. The pro-caspase-1 protein level was significantly decreased in 9-month DBA/2J, and the active form of caspase-1 (p20) significantly increased in 9-month DBA/2J (Figure 3.4 A-C). Correspondingly, GSDMD, the downstream substrate of p20, is significantly increased in the older DBA/2J group, which was well aligned with the p20 expression levels (Figure 3.4 D-E). These results confirmed that

inflammasome activation exists in the 9-month DBA/2J mouse eyes. However, there is a variation between biological repeats within the same group. Further details will be discussed in section 4.2.1.

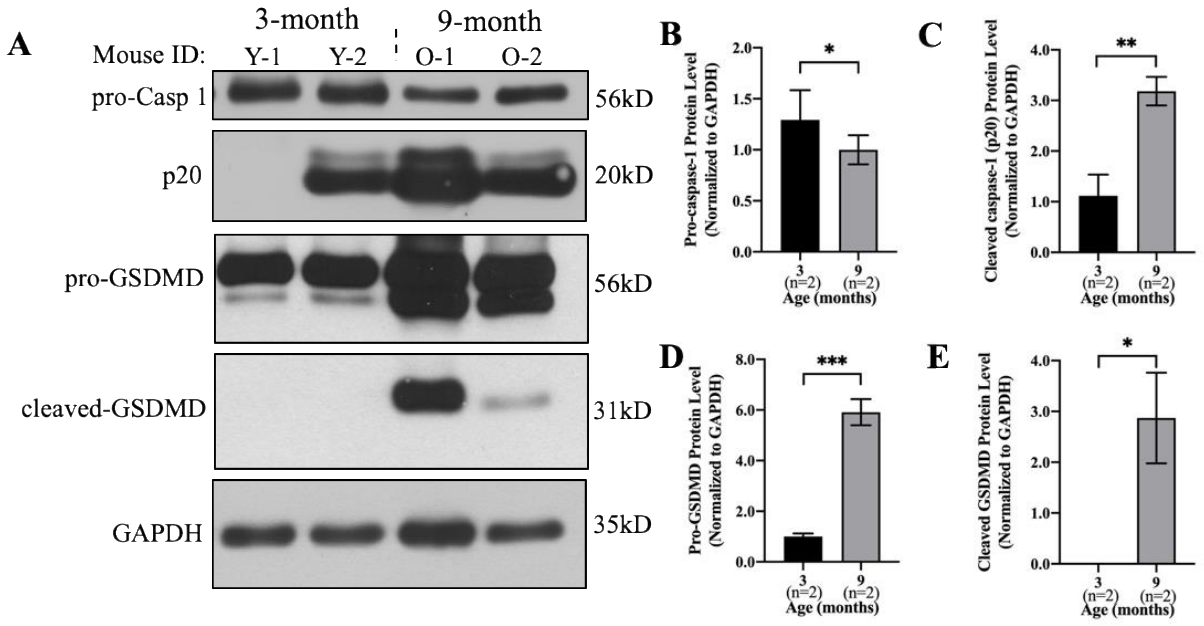

Figure 3.4 Western blot and analysis of 3-month and 9-month DBA/2J mice. Western blot pattern of gasdermin D (GSDMD) and caspase-1 on DBA/2J eye lysate (A) and quantification by image J and statistical analysis by Graphpad (B-E, t-test, MEAN±SEM, n=2, 1 eye/mouse, *p<0.05, **p<0.01, ***p<0.005; The value of the first column in E equals zero).

3.4 Correlation of IOP and NLRP3 inflammasome activity

To determine whether NLRP3 inflammasome activity is related to IOP elevation in aged DBA/2J eyes, we performed a linear regression analysis to correlate the IOP measurement of a single eye together with its cleaved caspase-1 protein expression level and NLRP3 immunolabeling level (Figure 3.5). The cleaved caspase-1 protein level and NLRP3 immunolabeling were significantly correlated to IOP level (R_2=0.5079, p=0.0093; R_2=0.6459,

p=0.0162 respectively). These results indicate that NLRP3 inflammasome activities are correlated with IOP levels in DBA/2J eyes.

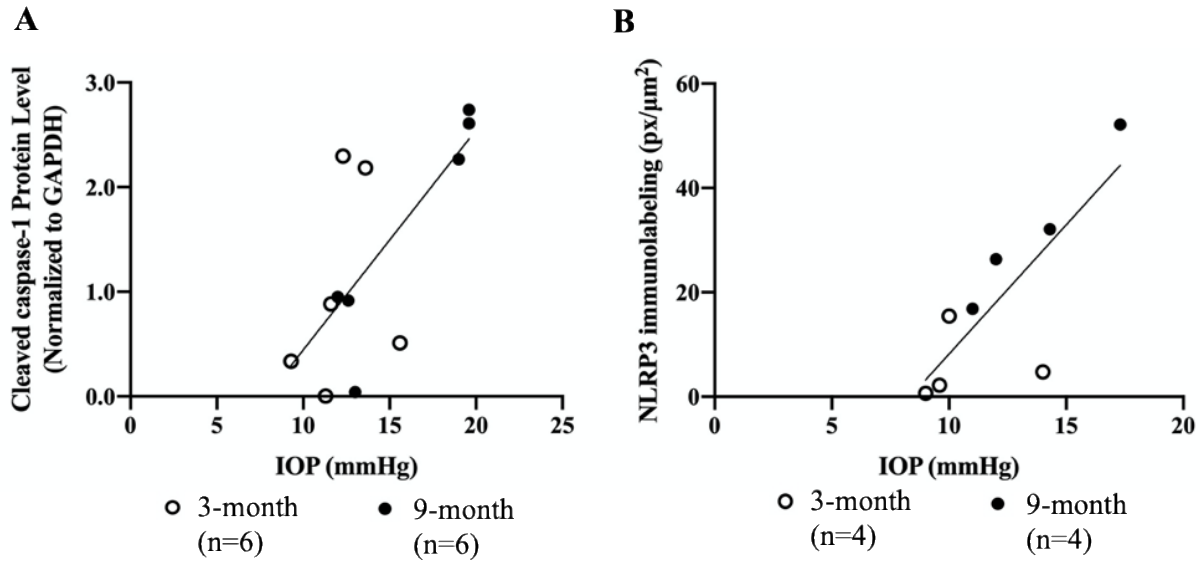

Figure 3.5 NLRP3 and cleaved caspase-1 expression level is correlated with IOP in DBA/2J model. Western blot density of cleaved caspase-1 (A) and IHC staining of NLRP3 (B) from untreated 3-month and 9-month old DBA/2J is plotted with corresponding IOP (A: Right eye IOP and cleaved caspase-1 protein level of 6 mice each from 3-month and 9-month group; B: Left eye IOP and NLRP3 immunolabeling of 4 mice each from 3-month and 9-month group). Linear regression analysis based on 95% confidence level, n=12, 1 eye/mouse, R^2=0.5079, p=0.0093(A); n=8, 1 eye/mouse, R^2=0.6459, p=0.0162 (B).

To further investigate this correlation between IOP and NLRP3 inflammasome activity, and to exclude the effect of aging, we used C57BL/6J as normal tension age-matched control. NLRP3 IHC immunolabeling were performed to compare the expression level of NLRP3 in C57BL/6J at 3 months and 9 months of age (Figure 3.6 A-D). A two-way ANOVA was conducted to examine the effect of age and retinal regions on NLRP3 immunolabelling. The result indicated that there was no effect of age or retinal regions on NLRP3 immunolabelling in

C57BL/6J (Figure 3.6, E). This result indicates that NLRP3 inflammasome expression level is independent of aging in C57BL/6J. Therefore, we could infer that NLRP3 inflammasome activity is correlated with IOP elevation in DBA/2J eyes.

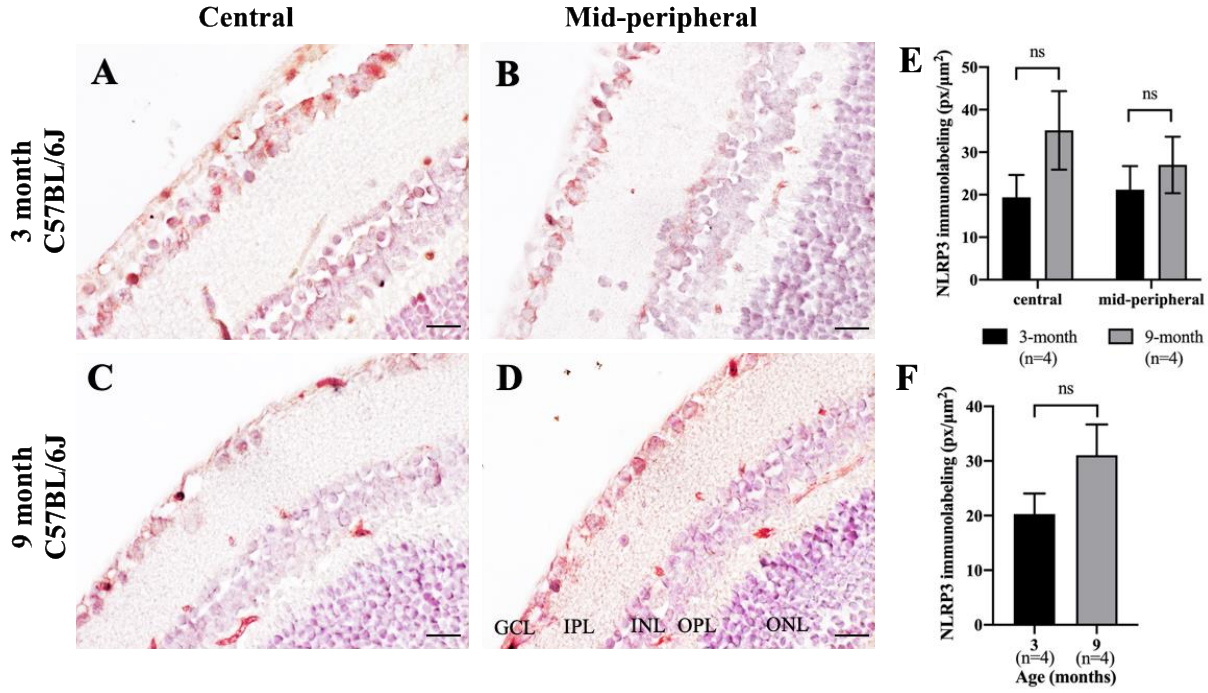

Figure 3.6 NLRP3 IHC staining on C57BL/6 retina. NLRP3(Cryo-2) IHC staining on 3 and 9 months of age C57BL/6J retina (A-D, red=NLRP3); corresponding NLRP3 labeling is quantified by pixel numbers of certain threshold (manually selected in photoshop, background eliminated by deselecting colors from negative control image) inside a fixed sample box (E). Total NLRP3 immunolabeling from both retinal regions were quantified and analyzed (F). Two-way ANOVA indicated no significant effect of age or retina regions on NLRP3 labelling [F (1,44) =0.52, p=0.47]. T-test indicated no significant difference in 3-and 9-month C57BL/6J. Mean ± SEM, n=4, 2 data points per retinal area per mouse, ns=not significant. GCL: ganglion cell layer; IPL: inner plexiform layer; INL: inner nuclear layer; OPL: outer plexiform layer; ONL: outer nuclear layer; Scale bar=10 μm.

3.5 Increased number of microglial cells are detected in 9-month DBA/2J

Microglia cells respond to DAMPs and can be recruited by inflammatory cytokines produced by NLRP3 inflammasome activation. Hence, we examined microglial cell number and activation status by IHC using an antibody against IBA-1, a specific microglia cell marker. The immunoreactivity is located in the inner plexiform layer (IPL) and inner nuclear layer (INL) (Figure 3.7 A, B). Both resting (ramified) and activated (amoeboid) microglia cells were observed in DBA/2J tissues at both age groups. However, the number of microglial cells in the 9-month DBA/2J group is significantly greater than the 3-month DBA/2J group (Figure 3.4 C), which suggests that more microglial cells might be recruited in older DBA/2J retina.

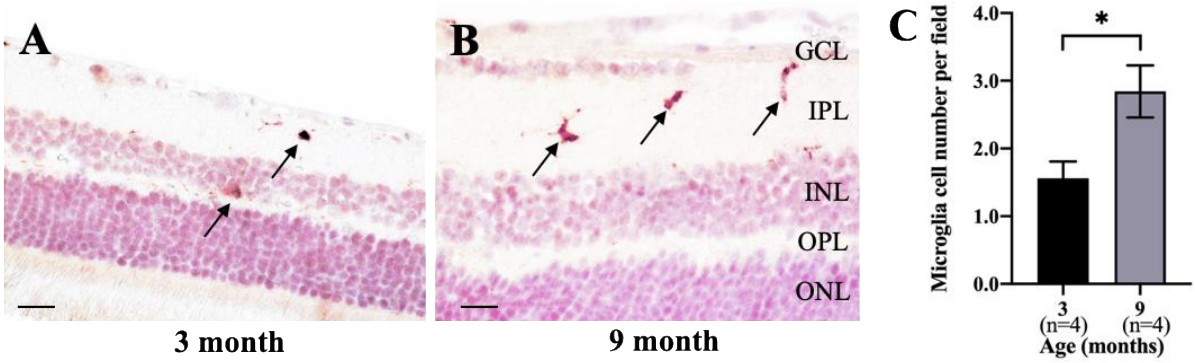

Figure 3.7 IBA-I IHC staining results on DBA/2J retina. IBA-1AEC labeling on 3-month and 9-month-old DBA/2J retina cross sections (A,B); Corresponding microglia cell number was manually counted under 20X Nikon Eclipse 80i microscope (C, Mann-Whitney test was used for statistical analysis, Mean ± SEM, n=4, 1 eye/mouse, **p<0.01.) GCL: ganglion cell layer; IPL: inner plexiform layer; INL: inner nuclear layer; ONL: outer nuclear layer. Scale bar=10 μm.

3.6 MCC950 oral administration

Multiple modes of drug administration are available for MCC950, including systemic (intraperitoneal injection, oral) and local (intraocular injection) methods. Given that intraocular injections are invasive and may induce local inflammation within the posterior chamber of the eye, which may subsequently confound the results, we chose systemic (oral) administration for these studies. Our pilot pharmacokinetic analysis of MCC950 (given by intraperitoneal injection every two days) suggests that the MCC950 levels in blood were essentially cleared within 24 hours (Figure A-1). Therefore, to maintain a sufficient drug level, we chose to use daily oral administration and increase the dosage to 30 ng/ml based on similar studies.[76] We observed that there was no difference of the drug metabolism rate between young and old DBA/2J mice. Daily oral administration resulted in drug levels approximately 7650±775 ng/ml in the serum and 370±109 ng/ml in the eye tissues (Figure 3.8). The earlier literature suggested that serum levels over 1000 ng/ml were therapeutically sufficient for lowering NLRP3 activity in several inflammatory disease models.[74]

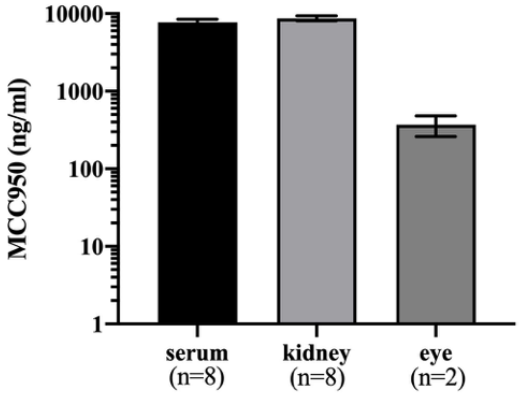

Figure 3.8 MCC950 concentration in treated DBA/2J. MCC950 concentration in serum, kidney and eye tissues at 6h after oral administration (MEAN±SEM, n=8 for serum and kidney, 1 kidney/mouse; n=2 for eye, 1 eye/mouse).

3.7 IOP remains unchanged during MCC950 treatment

During the 8-week treatment period, we examined the IOP of the DBA/2J mice in treatment and control groups. The result showed only a significant effect of age on IOP [$F(2,62)=9.558$, $p<0.001$], no significant effect on the interaction between age and treatment [$F(2,62)=1.071$, $p=0.3491$], and no significant difference between the treatment and control group [$F(1,62)=0.26$, $p=0.61$, Figure 3.9]. The result indicated that MCC950 did not affect IOP in DBA/2J eyes, a result that was consistent with the overall hypothesis that the elevation of IOP in aged DBA/2J eyes leads to the activation of the inflammasome, and not the reverse.

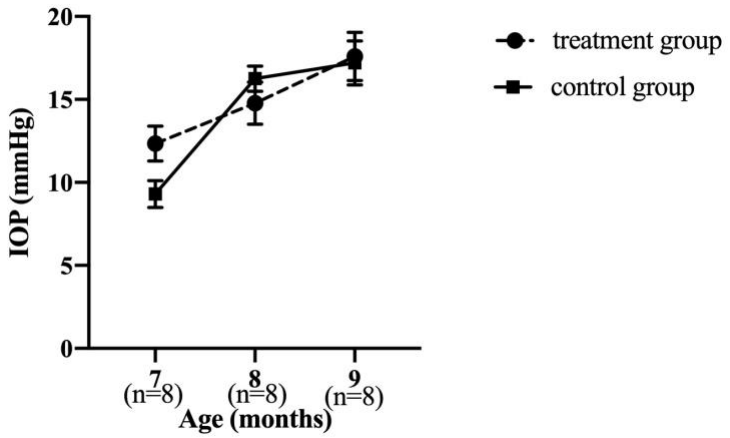

Figure 3.9 IOP measurement during 2 months of MCC950 treatment on DBA/2J. IOP of control group DBA/2J (solid square) and treatment group DBA/2J (solid circle) were measured at the same time of the day every two weeks during MCC950 treatment. Two-way ANOVA indicated a significant effect of age on IOP [F (2,62) =9.558, p<0.001], but no effect of treatment on IOP [F(1,62) =0.26, p=0.61]. (Mean±SEM, n=8, 2 eyes/mouse).

3.8 Reduced NLRP3 expression in treated DBA/2J retina and ciliary body

To examine whether MCC950 could successfully lower inflammasome activity in the retina, NLRP3 IHC was undertaken in retinal cross-sections from both treatment and control groups. The result of the control group demonstrated a similar pattern to that observed in the baseline study of 9-month DBA/2J. A two-way ANOVA was conducted to examine the effect of age and retinal regions on NLRP3 immunolabelling. There was a significant effect of treatment on NLRP3 immunolabelling [F (1,28) =6.62, p=0.015], while no effect of retinal regions [F (1,28) =0.336, p=0.56] (Figure 3.10). Bonferroni *post hoc* test indicated that the NLRP3 immunolabelling in mid-peripheral area of treated DBA/2J was significantly lower than control DBA/2J mice. Significantly decreased NLRP3 expression was also detected in the epithelial cells of the ciliary body of the treated DBA/2J comparing with the control group (Figure 3.11).

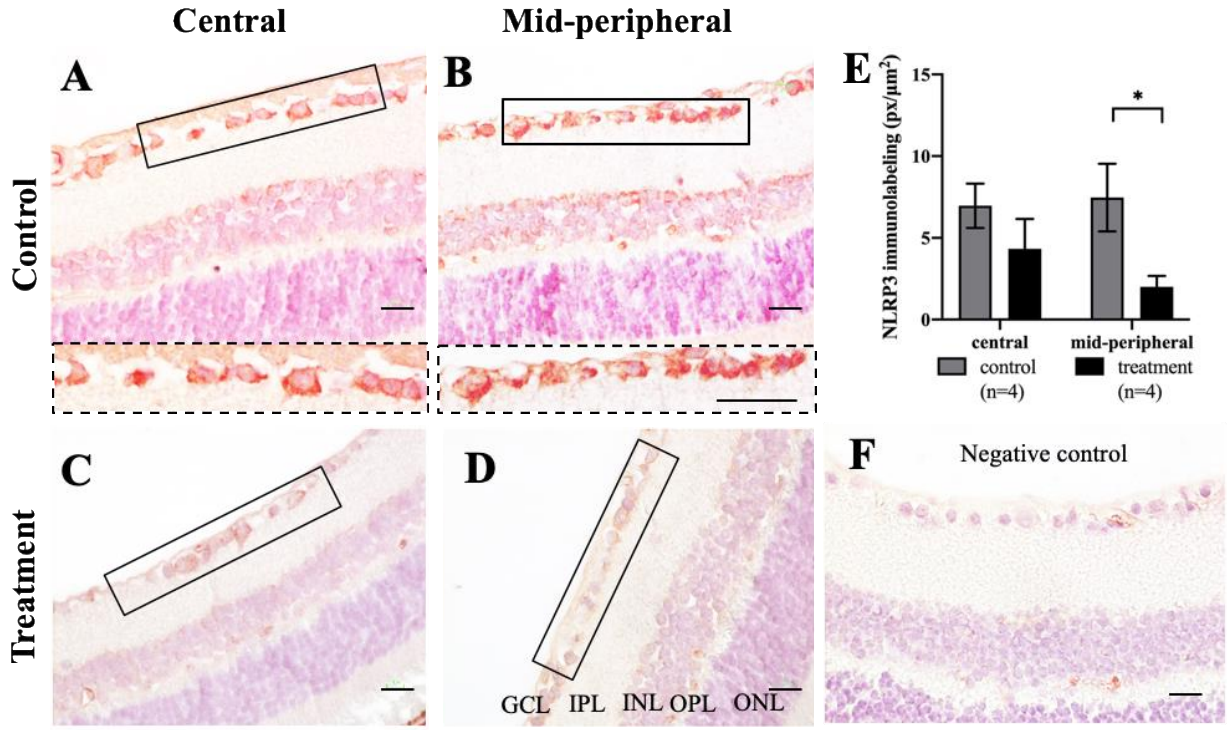

Figure 3.10 NLRP3 IHC staining on treated and control DBA/2J retina. NLRP3(Cryo-2) IHC staining on 9-month-old and treated DBA/2J mouse retinal ganglion cells (A-D, red=NLRP3); corresponding total NLRP3 staining is quantified by pixel numbers of certain threshold (manually selected in photoshop, background eliminated by deselecting colors from negative control image) inside a fixed-size sample box (indicated as the rectangle in A-D). Negative control of NLRP3 staining (IHC staining on DBA/2J cross-sections without primary antibody) (F). Two-way ANOVA indicated a statistically significant effect of treatment on NLRP3 labelling [$F(1,28)=6.62$, $p=0.015$], followed by Bonferroni's *post hoc* test (E, Mean ± SEM, n=4, 2 data points per retinal area per mouse, *$p<0.05$, **$p<0.01$). GCL: ganglion cell layer; IPL: inner plexiform layer; INL: inner nuclear layer; OPL: outer plexiform layer; ONL: outer nuclear layer;Scale bar=10 μm.

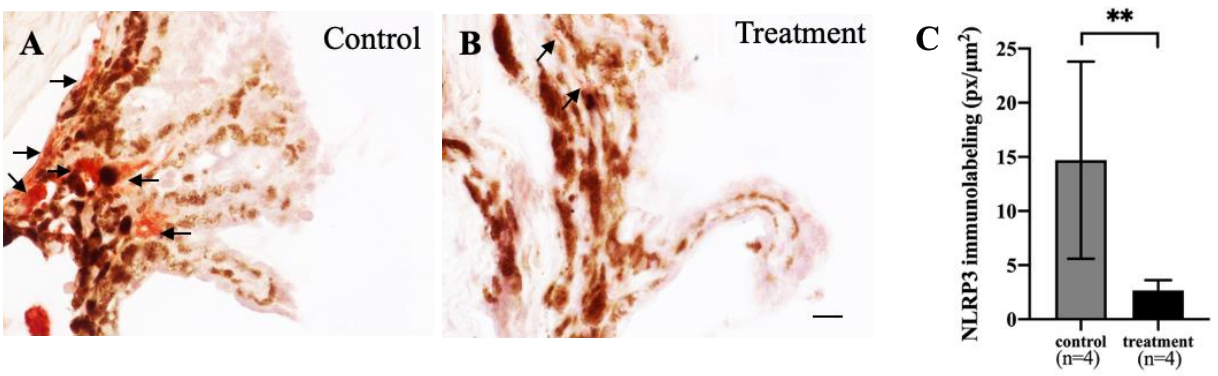

Figure 3.11 NLRP3 IHC staining on treated and control DBA/2J ciliary body. NLRP3 (Cryo-2) IHC staining on 9-month-old and treated DBA/2J mouse ciliary body (A-B, arrows); corresponding total NLRP3 staining is quantified by pixel numbers of certain threshold selected inside a fixed-size sample box. Mann-Whitney test is used for statistical analysis (C, Mean ± SEM, n=4, 1 eye/mouse, *p<0.05, **p<0.01). Scale bar=10 μm.

3.9 Reduced active caspase-1 expression in treated DBA/2J eyes

To further assess inflammasome activities, we examined the expression level of downstream products of activated NLRP3 inflammasome: caspase-1 and IL-18, through Western blot analysis (Figure 3.12 A). The result shows a decrease of p20 (Figure 3.12 C), which strongly indicates that inflammasome activity was successfully inhibited by MCC950 in the DBA/2J retina. To note, we observed that pro-caspase-1 was also higher in treatment group (Figure 3.12 B), which suggests that less pro-caspase-1 is cleaved in the treatment group, and this aligns with the reduced p20 band observed in treatment group. Additionally, if we combine the result showed in section 3.6 and Figure 3.9 (There was no change in IOP elevation with MCC950), we could conclude that inflammasome activity is not contributing to IOP elevation in DBA/2J eyes.

However, we failed to detect the IL-18 in the whole-eye lysate, presumably due to the relatively low level of secreted mature IL-18 in the protein lysate. Since pro-IL-18 precursor is

constitutively expressed, and the pro-IL-18 level of treatment group is higher than the control group (Figure 3.12 D), together with the result that cleaved caspase-1 is supressed in treatment group, we could reasonably infer that mature IL-18 production is suppressed in MCC950-treated DBA/2J eyes.

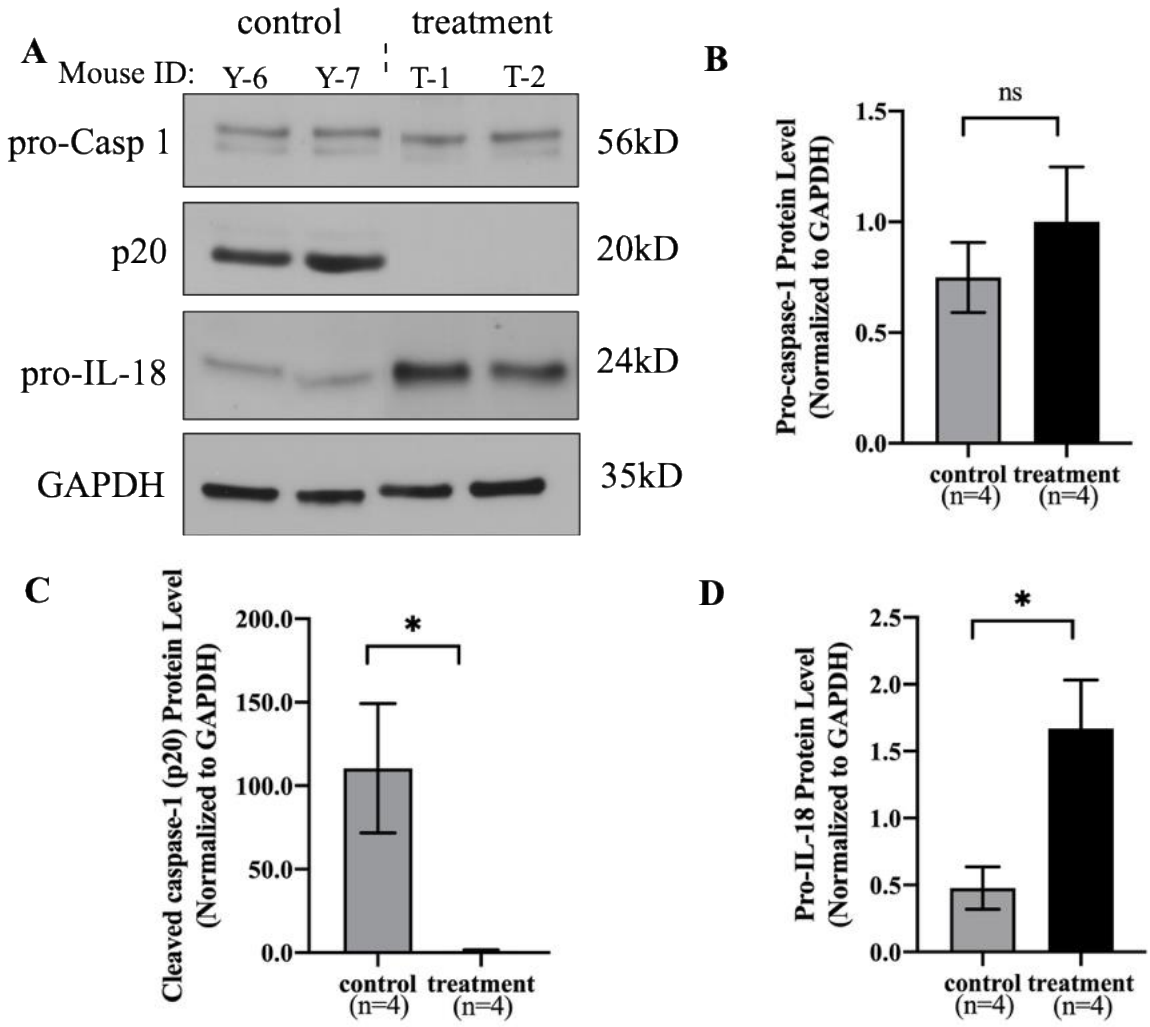

Figure.3.12 Western blot and analysis of control and MCC950-treated DBA/2J. Western blot pattern of IL-18 and caspase-1 on DBA/2J eye lysate (A) and quantification by image J (B-D, MEAN±SEM, n=4, 1 eye/mouse, *p<0.05)

3.10 Potential RGC rescue effect on mid-peripheral area of retina

To examine whether RGC survival is affected by inflammasome activation, we performed RBPMS (RNA-binding protein with multiple splicing, a specific RGC marker) immunofluorescence labeling on retina whole-mounts of 3, 9-month and MCC950-treated 9-month DBA/2J mice. The flat-mounted retina was divided into three areas: central retina, mid-peripheral retina and far-peripheral retina respectively according to their distance from the optic nerve head (Figure 3.13 A). A two-way ANOVA was conducted to examine the effect of age/treatment and retinal regions on RGC numbers. There was a significant interaction between age/treatment and retinal regions on RGC numbers [$F(4,121) = 5.065$, $p<0.001$]. For the central areas, there was no significant difference between 3-month DBA/2J (778.1±84.83 cell/mm^2), 9-month DBA/2J (712.5±129.7 cell/mm^2) and MCC950-treated 9-month DBA/2J (596.4±46.98 cell/mm^2), same for the far-peripheral areas. However, the Tukey's *post hoc* test indicated that in the mid-peripheral area, there was a significant decrease in RGC number in the 9-month DBA/2J retina (480.3±84.89 cell/mm^2) comparing to 3-month DBA/2J retina (1024±57.66 cell/mm^2). The treatment group showed an increase in number of RGCs (767.7±81.88 cell/mm^2) compared to the 9-month (untreated) group. This result suggests that MCC950 suppressed RGC loss in the mid-peripheral retina was presumably due to the drug's ability to inhibit NLRP3 inflammasome activity.

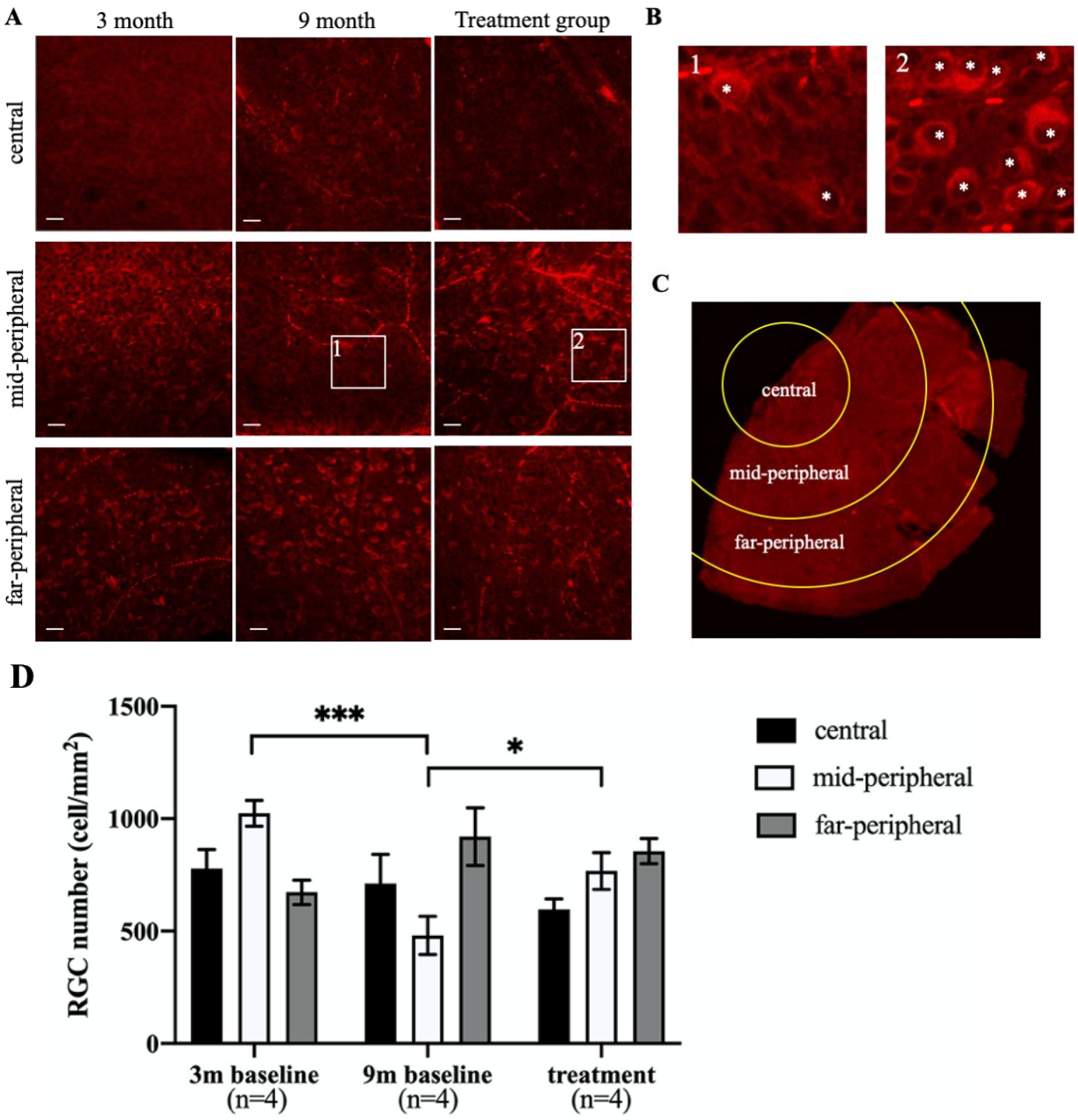

Figure 3.13 Immunofluorescent staining for RGCs of whole-mount eye cup of DBA/2J. RGCs in different areas of retina under 20X confocal microscope. Red=RBPMS immunoreactivity (A). Enlargement of boxed area 1 and 2 (B), asterisk=counted RGCs. Area of wholemount retina identifying the division of the retina into central, mid-peripheral and far-peripheral view (C). Two-way ANOVA indicated a significant interaction between the effects of age and retinal regions on RGC numbers [$F(4,121) = 5.065$, $p<0.001$], followed by Tukey's *post hoc* test (D) MEAN±SEM, n=4, 4 data points per retinal area per mouse, ***$p<0.001$, *$p<0.05$). Scale bar=10 μm.

3.11 Microglia cell numbers remains unchanged in treated DBA/2J retina

Having detected the reduction of active caspase-1 and inflammasome activity, we then checked the microglial cell counts by IBA-1 IHC after drug treatment. However, the total number of microglial cells did not change as our expectation (Figure 3.14). The total number of microglial cells remained the same in the control (14.25±1.15 cell/20X microscope field) and treatment groups (13.25±1.56 cell/20X microscope field).

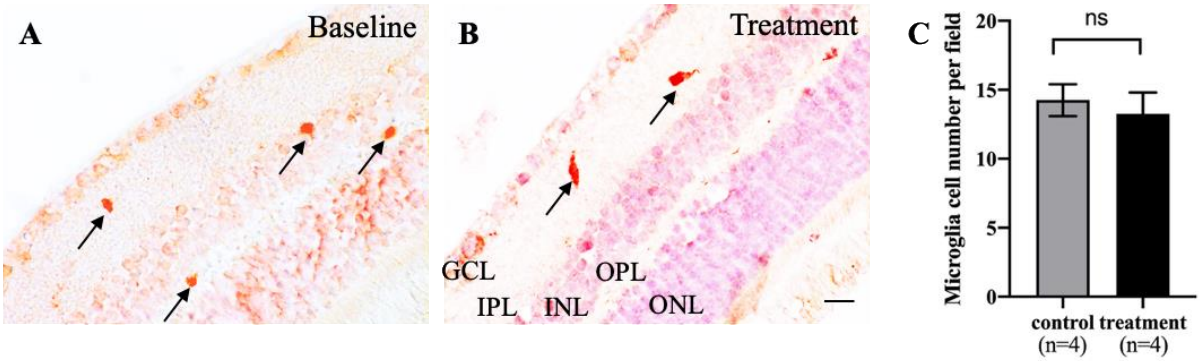

Figure 3.14 IBA-1 IHC staining on control and MCC950-treated DBA/2J. IBA-1 AEC staining on 9-month control and treated DBA/2J retina cross sections (A); Corresponding microglia cells count per visual field under 20X Nikon Eclipse 80i microscope (B). T-test was used for statistical analysis. (Mean ± SEM, n=4, 1 eye/mouse). Scale bar=10 μm

Chapter 4: Discussion

4.1 Aim 1: Activation of the NLRP3 inflammasome during aging and IOP elevation

The first aim of this study was to determine whether the activation of the NLRP3 inflammasome changes during aging and IOP elevation in DBA/2J retina. We monitored IOP and NLRP3 inflammasome activity in young and old DBA/2J. We observed IOP elevation increase from 3 months to 9 months of age (Figure 3.1). We also observed NLRP3 inflammasome expression increase in the retinal ganglion cell layer (Figure 3.2) and in ciliary epithelium (Figure 3.3) as described in result session 3.1-3.4.

4.1.1 Elevation of IOP during aging

In this study, we observed an elevation of IOP in DBA/2J with aging. According to the literature, the IOP begins to elevate at 6 months of age and peaks at 9 months of age in DBA/2J mice.[82] Our result of IOP changes in DBA/2J is consistent with the literature. The IOP of 9-month DBA/2J mice also exhibited a relatively high variance compared to other age groups, which is consistent with the original study describing the ocular changes in this mouse model.[82] The variation in IOP could potentially indicate a difference in pigmentary glaucoma disease progression in individual animals. As Howell et al. described, DBA/2J at 10 months of age displayed different severity of glaucoma, and they further divided them into 5 stages through molecular clustering.[83] This suggests a variation at the molecular level and/or in the breakdown of the iris (e.g., disease progression) in individual DBA/2J mice of the same age.

4.1.2 NLRP3 expression in DBA/2J RGCs during aging

In our NLRP3 IHC analysis, we detected a majority of NLRP3 positive staining in the RGCs (Figure 3.2), which suggested NLRP3 inflammasome expression in retinal ganglion cells (a neuronal cell type). From the literature we know that the NLRP3 inflammasome complexes are present in immune cells such as microglial cells and astrocytes.[103-104] There are limited data to support that the NLRP3 inflammasome complexes are also expressed by neurons.[105-106] Abulafia et al detected caspase-1 expression in spinal cord neurons in thromboembolic stroke study,[107] and Rivero Vaccari et al. demonstrated NLRP1 inflammasome exists in neurons, together with caspase-1, pro-IL-18 and pro-IL-1β.[108] They also demonstrated that neurotoxicity was facilitated by neuronal inflammasome activity in a spinal cord injury model.[109] In recent studies, Pronin et al demonstrated the activation of NLRP3 inflammasome is detected in RGCs and astrocytes exposed to the hypertension stress. [37] These findings in literature support the idea that the inflammasome pathway could be activated in neuronal cells. Thus, our findings may reveal a new avenue of investigation into NLRP3 inflammasome activity in retinal neurons in DBA/2J model as it pertains to retinal degenerations. *In vitro* experiments such as RGC purification and culture may be performed to further address this question.[110]

4.1.3 NLRP3 inflammasome activity in ciliary body

We detected NLRP3 expression in the epithelial cells of the ciliary body (Figure 3.3). This result indicates NLRP3 inflammasome activity in the ciliary body epithelium in this hypertensive mouse model, which is a novel finding of our study not yet reported in the literature. We could reasonably infer from the literature that an inflammatory response is associated with pigment dispersion syndrome. In pigment dispersion syndrome, the pigments

dispersed from the degradation/atrophy of the iris could precipitate and clog the trabecular meshwork and ciliary body, and lead to an abnormal response of intraocular immune system. Alternatively, the dispersed pigments may disrupt the immune privilege of the eye, which may lead to infiltration of immune cells.[89, 111] The infiltrated immune cells may be recruited at the ciliary epithelium and provide a platform for NLRP3 inflammasome activation. Studies have demonstrated that IL-18 is constitutively expressed by ciliary body epithelium cells in animal model of experimental autoimmune uveitis and DBA/2J.[112-113] Although we did not locate the expression pattern of IL-18 in the DBA/2J retina, the increased NLRP3 expression at the ciliary body may support this idea in literature.

Another study demonstrated that inflammation can cause ciliary body shutdown, leading to reduced aqueous production.[114] To better understand the changes of ciliary body undergoing elevated IOP, it would be worthwhile to study the dynamics of aqueous humor of DBA/2J.[115] We could infer from the literature that reduced production of aqueous humor leads to the reduction of IOP. However, both in the literature and in our study, we did not observe a decrease in IOP with aging, even though there was inflammation in the ciliary body due to NLRP3 inflammasome activities. The remaining of high IOP is possibly due to the unchanged the outflow resistance of TM. When the TM is still having a high resistance, the aqueous humor continues accumulating within the eye (the outflow rate is lower than the production rate), thus the elevation of IOP remains unchanged. In contrast to the literature in which uveitis may lead to secondary glaucoma and ocular hypertension,[116] in hypertensive eyes in DBA2J it might suggest that the elevated IOP may also possibly lead to inflammation in ciliary body.

4.2 Aim 2: Activation of the NLRP3 inflammasome due to elevated IOP

The second aim of this study is to determine whether NLRP3 inflammasome is activated by elevated IOP in DBA/2J mouse model. As addressed in the previous session, NLRP3 inflammasome expression is increased together with aging and elevated IOP. These results are further discussed in this section in order to understand the relationship between IOP and NLRP3 inflammasome better.

4.2.1 Aging, IOP and NLRP3 inflammasome activity correlation

During our protein expression measurements of NLRP3 (from IHC immunolabeling), we found a large variance between individual animals within the same group. We also observed differences of IOP and a distinct level of caspase-1 expression level between animals within the same age group. In our hypothesis, inflammasome activity is triggered by IOP elevation. Therefore, we performed a linear regression analysis to correlate the IOP measurement of a single eye together with its protein expression level, and we found that the caspase-1 cleavage and NLRP3 expression level is significantly related to IOP level.

Next, we studied 3-and 9-month old wild-type mice C57BL/6J. Importantly, earlier studies indicated that the IOP remains constant (ranging from 7-12 mmHg for 3 to 9 month-old C57BL/6J mice) during aging.[91] Another study carried out by Savinova et al.[101] indicated that IOP level decreases with age (13 mmHg for 3- to 12-month mice and 10 mmHg for 24-month mice) in C57BL/6J. We performed NLRP3 IHC staining and demonstrated that there's no difference of NLRP3 expression between 3-month and 9-month C57BL/6J. These results indicate that NLRP3 is not affected by aging in C57BL/6J mouse strain, and it remains constant when IOP was not elevated.

NLRP3 inflammasome expression increases in aged DBA/2J and remains unchanged in aged C57BL/6J. These results are consistent with the hypothesis that NLRP3 activity increases with elevated IOP, and this appears to be independent of age. Therefore, we could infer that NLRP3 inflammasome activity is associated with elevated IOP. A possible mechanism behind this association is that NLRP3 inflammasome responds to ischemia injury caused by elevated IOP. As Wei et al demonstrated, High-mobility group box 1 (HMGB1), an abundant protein involved in several inflammatory diseases, mediates ischemia-associated inflammatory response by activating NLRP3 inflammasomes as DAMP in an acute glaucoma model.[117] Thus, we could infer that HMGB1 may also play a role in chronic glaucoma models. Further studies are needed to address the detailed mechanism of what triggers the activity of the inflammasome during IOP elevation.

4.3 Aim 3: NLRP3 inflammasome activity contributes to RGC death

The third aim of the study is to determine whether NLRP3 inflammasome contributes to RGC death in DBA/2J mouse model. We hypothesize that NLRP3 inflammasome activation leads to RGC death, and by inhibiting the NLRP3 inflammasome with MCC950, RGC death will be reduced.

4.3.1 NLRP3 activity and RGC loss are reduced by MCC950 treatment

Inflammasome activity was increased in DBA/2J retina at 9 months of age, indicated by the upregulation of NLRP3 and cleaved caspase-1 expression levels (Figure 3.2-3.4). This was expected because of elevated IOP and reduced RGC numbers in 9-month DBA/2J.

NLRP3 inflammasome activity is also associated with RGC loss in the mid-peripheral area of the retina. Interestingly, earlier reports indicate that spontaneous RGC loss begins in the mid-peripheral area of the retina then tends to shift toward the ONH (centre of the retina) in later ages, with the far-peripheral area relatively preserved.[118] The treatment study successfully confirmed our hypothesis, that MCC950 could reduce NLRP3 expression and caspase-1 cleavage by inflammasome activity.

Furthermore, in the treatment study we also demonstrated that MCC950 administration did not affect IOP levels of DBA/2J. Hence, we could further conclude that reducing inflammasome activity does not lower IOP in DBA/2J mouse model, and therefore the rescue of the RGC in the mid-peripheral retina appears to be due to the lowering of inflammasome activity without lowering IOP. These findings are in contrast to the hypothesis proposed by Wilson et al,[93] who suggested IOP is induced by inflammation early in the young DBA/2J mice. More details about the relationship of IOP and inflammasome activation are discussed in section 4.6.

4.3.2 The mechanism of MCC950 reducing NLRP3 expression

Notably the mechanism behind MCC950 inhibitory effect is its binding affinity to NACHT domain on the NLRP3 protein, which eliminates the ATPase function of NACHT and prevents the NLRP3-ASC oligomerization.[75] The precise mechanism of how it results in lowering expression level of NLRP3 in the peripheral retina of 9-month DBA/2J is still unclear as it is not consistent with the presumed mechanism of MCC950.

We may speculate that (as described as Figure 4.1) the stress induced by increased IOP in aged DBA/2J eyes promotes inflammasome activity in RGCs which possibly leads to cell death. The DAMPs released from the death of RGCs and the cytokines IL-18/IL-1β produced by

inflammasome bind to the TLR and IL-18/IL-1β receptors on the cell surface of adjacent RGCs, which further promote NLRP3 transcription through NF-kB pathway and result in the upregulation of NLRP3 expression level. These events may also accelerate the RGC death process, or in other words, as RGCs die due to elevated IOP, this results in a positive feedback in provoking the NLRP3 inflammasome pathway, which would result in more cell death. Thus, suppressing of NLRP3 inflammasome activation could decelerate or even stop this process.

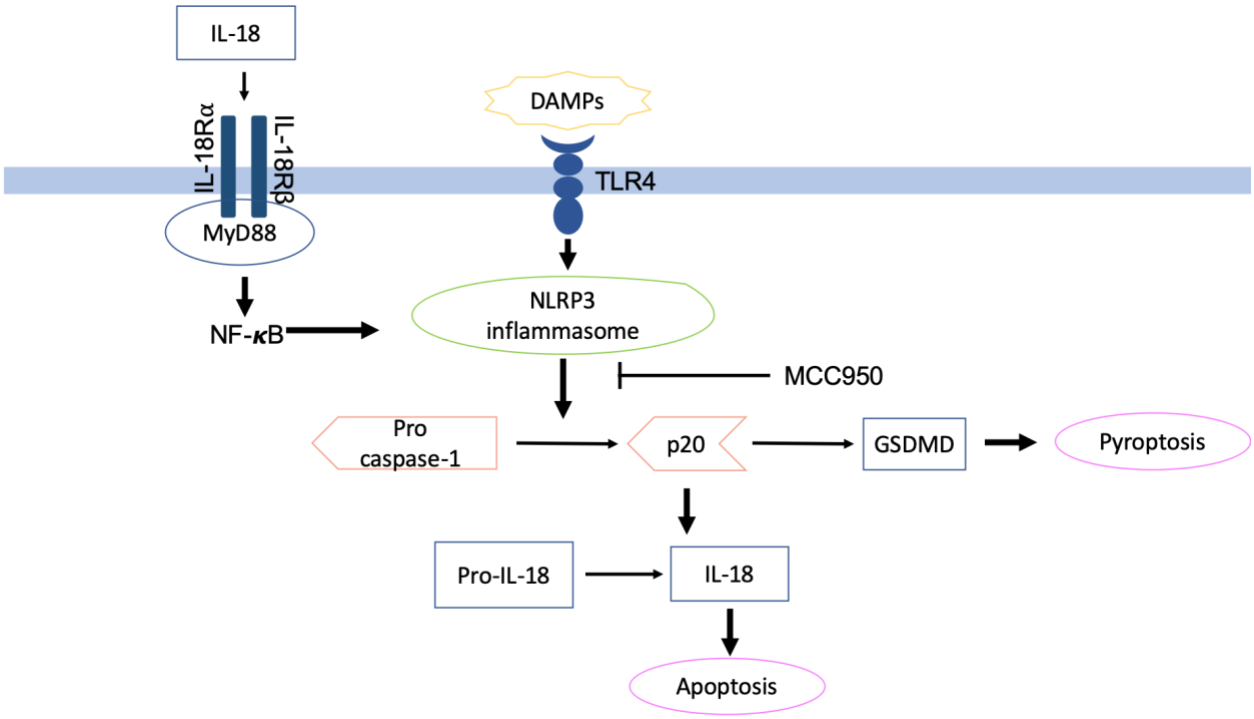

Figure 4.1 Schematic diagram of NLRP3 inflammasome and RGC death. NLRP3 inflammasome is activated by DAMPs (death/damage associated molecule pattern) released by necrotic cells, and subsequently cleave pro-caspase-1 into active caspase-1 (p20). Active caspase-1 then cleaves pro-IL-18 into its mature form (active IL-18). The released pro-inflammatory cytokine will bind to IL-18R (IL-18 receptors) on the surface of other cells, then trigger NF-kB pathway, therefore promote the gene transcription of NLRP3 inflammasome and accelerate cell death. Another substrate downstream of active caspase-1 is gasdermin d (GSDMD) that promotes cell pyroptosis through por-formation on cell membrane.

4.4 Limitation of the study

Our primary objective was to determine whether NLRP3 inflammasome activity contributes to RGC loss during glaucoma pathogenesis. We showed that MCC950 can reduce RGC loss in DBA/2J mice. However, we do not yet know whether RGC death is due to pyroptosis mediated by activated GSDMD. We were unable to confirm that the rescue of RGC was due to the prevention of pyroptosis, since the assay of GSDMD (which introduces pore formation on the membrane surface, as a marker for pyroptosis) was technically challenging. Whether RGCs undergo pyroptosis during elevated IOP remains to be determined. Alternative ways to address this remaining question are through fluorochrome inhibitor of caspases assay (FLICA) on frozen retina. FLICA kits could measure apoptosis by detecting active caspases in whole-living cells and frozen tissues. The regent contains a caspase-1 inhibitor and a fluorescent probe for detecting active caspases. Further attempts are needed to assess the precise mechanism behind RGC loss.

Note that in the study we used NLRP3 IHC to locate inflammasome proteins to RGCs. However, we assessed active caspase-1 by western blot as an indicator of inflammasome activity, but with whole eye lysate. We could not separate RGCs for protein lysates. To better locate and visualize NLRP3 inflammasome oligomerization in related cells (RGCs or microglial cells), immunofluorescence staining of ASC specks (a specific morphological change of ASC during inflammasome assembly) may be performed.

Since we were unable to detect the mechanism behind RGC death, our finding is only a preliminary result that reveals the association of NLRP3 inflammasome and RGC loss. Unfortunately, the amount of protein lysate from one mouse eye is relatively limited, it is unable to integrate the protein lysate from multiple animals to enhance the signal. In addition, gathering

protein lysate from more than one animal (pooling the samples) may be problematic due to the high variations of disease progression and IOP between individual animals of the same age group.

We used C57BL/6 as the normal tension control animal, however this mouse strain is not genetically identical to DBA/2J, which may induce potential contingencies. To better assess this problem, a more proper control animal may be introduced, for instance the *Gpnmb+ DBA/2J* mouse strain, which does not gain IPD phenotype and hypertension because of the *Gpnmb* heterozygotes. Alternatively, using pressure lowering drops in the DBA2J mouse may allow additional insights into the role of IOP elevation and inflammasome activation. As Wong et al demonstrated, 0.25%-0.5% Timoptic-XE could successfully reduce IOP in DBA/2J mice at 9-12 months of age with a rescue of RGC loss.[90] This is consistent with our finding that IOP induces RGC loss (mediated by inflammasomes).

4.8 Future Directions

We have concluded that inflammasome activities are associated with aging, and it contributes to RGC death in the DBA/2J glaucoma model. Our result suggests that inflammasome activity is upregulated with aging and concomitant increase in IOP in DBA/2J mice, and the question left behind is the precise trigger of inflammasome. NLRP3 requires a priming signal and an activation signal to become active. Under a sterile inflammation environment, the priming signals are typically DAMPs mediated by TLRs and IL-1Rs. According to the literature, high mobility group box 1 (HMGB1) protein are released by damaged neurons during neuroinflammation[119], and could bind to TLR receptors then subsequently activate NL-kB pathway and achieve inflammasome priming which is evident in a

rat neuroinflammation model[120]. For the activation signal, there's also several candidates including PAMPs mediated by potassium efflux channels. To note that P2X7 channel is dysfunctional in DBA/2J due to the *p2x7r* gene mutation.

In spite of RGCs, it is also important to examine the neuronal axons from the optic nerve head along the visual projection. A robust way to validate neuron numbers is by paraphenylenediamine staining (PPD staining). PPD stains myelin sheath of healthy neuron axons, and the neurons require resin-embedding and cross sectioned at 1 μm thickness. Examining the condition of RGC axons helps us better understand the mechanism of RGC loss and the role of inflammasome in this study.

Our study revealed that MCC950 worked successfully in inhibiting NLRP3 inflammasomes and rescued a subset of RGC loss in DBA/2J mouse model. It is important to continue to validate this small molecule inhibitor as a drug targeting inflammatory diseases. Experiments should be conducted to assess the mechanisms and side effects of this drug. More importantly, although the DBA/2J mouse strain is a widely used hypertensive model in glaucoma studies, it may have a different pathway than observed in human POAG and PACG, therefore more samples from human donors are needed to confirm whether they have common inflammatory pathway involved.

Chapter 5: Conclusion

In this study, our data revealed an upregulation of NLRP3 expression in RGCs and ciliary epithelium cells of 9-month DBA/2J mice with elevated IOP. IBA-1, a marker of microglia, also demonstrates an age-related increase. Western blot analysis on whole globe revealed greater cleaved caspase-1 and cleaved GSDMD in 9-month DBA/2J compared to 3-month DBA/2J mice. By treating the mice with MCC950, a small molecule NLRP3 inhibitor, caspase-1 cleavage was remarkably reduced. This result suggests MCC950 could successfully suppress NLRP3 inflammasome activity. RGCs at the mid-peripheral area of retina were rescued by MCC950 treatment. Therefore, we conclude that NLRP3 inflammasome activation contribute to RGC death in DBA/2J mice with elevated IOP. We further conclude that MCC950 treatment could inhibit NLRP3 inflammasome activity in DBA/2J eyes, thereby prevent RGC death.

References

1. *World Health Organization. Visual impairment and blindness. (Accessed in 2020)* *https://www.who.int/news-room/fact-sheets/detail/blindness-and-visual-impairment*.
2. Weinreb, R.N., T. Aung, and F.A. Medeiros, *The pathophysiology and treatment of glaucoma: a review.* JAMA, 2014. **311**(18): p. 1901-11.
3. Quigley, H.A. and A.T. Broman, *The number of people with glaucoma worldwide in 2010 and 2020.* Br J Ophthalmol, 2006. **90**(3): p. 262-7.
4. Tham, Y.C., et al., *Global prevalence of glaucoma and projections of glaucoma burden through 2040: a systematic review and meta-analysis.* Ophthalmology, 2014. **121**(11): p. 2081-90.
5. NationalEyeInstitute, *https://www.nei.nih.gov/learn-about-eye-health/eye-conditions-and-diseases/glaucoma*.
6. Fechtner, R.D. and R.N. Weinreb, *Mechanisms of optic nerve damage in primary open angle glaucoma.* Surv Ophthalmol, 1994. **39**(1): p. 23-42.
7. Goel, M., et al., *Aqueous humor dynamics: a review.* The open ophthalmology journal, 2010. **4**: p. 52.
8. Tielsch, J.M., et al., *Racial variations in the prevalence of primary open-angle glaucoma. The Baltimore Eye Survey.* JAMA, 1991. **266**(3): p. 369-74.
9. Klein, B.E., et al., *Prevalence of glaucoma. The Beaver Dam Eye Study.* Ophthalmology, 1992. **99**(10): p. 1499-504.
10. Salmon, J.F., *Predisposing factors for chronic angle-closure glaucoma.* Prog Retin Eye Res, 1999. **18**(1): p. 121-32.
11. Porter, D. *Chronic Angle-Closure Glaucoma Causes, Risk and Diagnosis*. 2019 [cited 2020.
12. Wang, N., et al., *Orbital cerebrospinal fluid space in glaucoma: the Beijing intracranial and intraocular pressure (iCOP) study.* Ophthalmology, 2012. **119**(10): p. 2065-2073 e1.
13. Killer, H.E. and A. Pircher, *Normal tension glaucoma: review of current understanding and mechanisms of the pathogenesis.* Eye (Lond), 2018. **32**(5): p. 924-930.
14. Merayo-Lloves, J., et al., *Secondary glaucoma in patients with uveitis.* Ophthalmologica, 1999. **213**(5): p. 300-4.
15. Niyadurupola, N. and D.C. Broadway, *Pigment dispersion syndrome and pigmentary glaucoma--a major review.* Clin Exp Ophthalmol, 2008. **36**(9): p. 868-82.
16. Kalogeropoulos, D. and V.C. Sung, *Pathogenesis of Uveitic Glaucoma.* J Curr Glaucoma Pract, 2018. **12**(3): p. 125-138.
17. Rodrigues, G.B., et al., *Neovascular glaucoma: a review.* Int J Retina Vitreous, 2016. **2**: p. 26.
18. Bussel, II, G. Wollstein, and J.S. Schuman, *OCT for glaucoma diagnosis, screening and detection of glaucoma progression.* Br J Ophthalmol, 2014. **98 Suppl 2**: p. ii15-9.
19. Narayanaswamy, A., et al., *A randomized, crossover, open label pilot study to evaluate the efficacy and safety of Xalatan in comparison with generic Latanoprost (Latoprost) in subjects with primary open angle glaucoma or ocular hypertension.* Indian J Ophthalmol, 2007. **55**(2): p. 127-31.

20. Bacharach, J., et al., *Double-masked, randomized, dose-response study of AR-13324 versus latanoprost in patients with elevated intraocular pressure.* Ophthalmology, 2015. **122**(2): p. 302-7.
21. Hennessy, A.L., et al., *Videotaped evaluation of eyedrop instillation in glaucoma patients with visual impairment or moderate to severe visual field loss.* Ophthalmology, 2010. **117**(12): p. 2345-52.
22. *Glaucoma Research Foundation-Glaucoma medications and their side effects; Reviewed on 2018.*
23. Rosin, L.M. and N.P. Bell, *Preservative toxicity in glaucoma medication: clinical evaluation of benzalkonium chloride-free 0.5% timolol eye drops.* Clin Ophthalmol, 2013. **7**: p. 2131-5.
24. Sakurai, Y., et al., *Chronic chorioretinal detachment under normal intraocular pressure in eye with uveitic glaucoma after trabeculectomy: A case report.* Medicine (Baltimore), 2020. **99**(2): p. e18652.
25. Investigators, A., *The Advanced Glaucoma Intervention Study: 8. Risk of cataract formation after trabeculectomy.* Arch Ophthalmol, 2001. **119**(12): p. 1771-9.
26. Rudnicka, A.R., et al., *Variations in primary open-angle glaucoma prevalence by age, gender, and race: a Bayesian meta-analysis.* Invest Ophthalmol Vis Sci, 2006. **47**(10): p. 4254-61.
27. Guedes, G., J.C. Tsai, and N.A. Loewen, *Glaucoma and aging.* Curr Aging Sci, 2011. **4**(2): p. 110-7.
28. Xu, X.H., et al., *Association between glaucoma and the risk of Alzheimer's disease: A systematic review of observational studies.* Acta Ophthalmol, 2019. **97**(7): p. 665-671.
29. Anat, L., B. Inbal, and S. Michael, *The retina as a window to the brain--from eye research to CNS disorders.* Nature Reviews Neurology, 2013. **vol. 9, no. 1**.
30. Zhang, C., T.T. Lam, and M.O. Tso, *Heterogeneous populations of microglia/macrophages in the retina and their activation after retinal ischemia and reperfusion injury.* Exp Eye Res, 2005. **81**(6): p. 700-9.
31. Hildebrand, G.D. and A.R. Fielder, *Anatomy and physiology of the retina*, in *Pediatric retina*. 2011, Springer. p. 39-65.
32. Fan, N., et al., *Measurement of photoreceptor layer in glaucoma: a spectral-domain optical coherence tomography study.* J Ophthalmol, 2011. **2011**: p. 264803.
33. Kolb, H., *Simple anatomy of the retina by Helga Kolb.* Webvision: The Organization of the Retina and Visual System, 2011.
34. Soto, I.H., G.R, *The Complex Role of Neuroinflammation in Glaucoma.* Cold Spring Harb Perspect Med, 2014.
35. Tezel, G., et al., *An astrocyte-specific proteomic approach to inflammatory responses in experimental rat glaucoma.* Invest Ophthalmol Vis Sci, 2012. **53**(7): p. 4220-33.
36. Howell, G.R., et al., *Radiation treatment inhibits monocyte entry into the optic nerve head and prevents neuronal damage in a mouse model of glaucoma.* J Clin Invest, 2012. **122**(4): p. 1246-61.
37. Pronin, A., et al., *Inflammasome Activation Induces Pyroptosis in the Retina Exposed to Ocular Hypertension Injury.* Front Mol Neurosci, 2019. **12**: p. 36.
38. Zhou, R. and R.R. Caspi, *Ocular immune privilege.* F1000 biology reports, 2010. **2**.

39. Benhar, I., *A London, and M Schwartz (2012) The privileged immunity of immune privileged organs: The case of the eye.* Front Immunol. **3**: p. 296.
40. Niederkorn, J.Y. and J. Stein-Streilein, *History and physiology of immune privilege.* Ocular immunology and inflammation, 2010. **18**(1): p. 19-23.
41. Graeber, M.B. and W.J. Streit, *Microglia: immune network in the CNS.* Brain Pathol, 1990. **1**(1): p. 2-5.
42. Lampron, A., A. Elali, and S. Rivest, *Innate immunity in the CNS: redefining the relationship between the CNS and Its environment.* Neuron, 2013. **78**(2): p. 214-32.
43. Zhu, H., et al., *An efficient delivery of DAMPs on the cell surface by the unconventional secretion pathway.* Biochem Biophys Res Commun, 2011. **404**(3): p. 790-5.
44. Liddelow, S.A., et al., *Neurotoxic reactive astrocytes are induced by activated microglia.* Nature, 2017. **541**(7638): p. 481-487.
45. Agudo, M., et al., *Immediate upregulation of proteins belonging to different branches of the apoptotic cascade in the retina after optic nerve transection and optic nerve crush.* Invest Ophthalmol Vis Sci, 2009. **50**(1): p. 424-31.
46. Krizaj, D., et al., *From mechanosensitivity to inflammatory responses: new players in the pathology of glaucoma.* Curr Eye Res, 2014. **39**(2): p. 105-19.
47. Lu, W., et al., *The P2X7 receptor links mechanical strain to cytokine IL-6 up-regulation and release in neurons and astrocytes.* J Neurochem, 2017. **141**(3): p. 436-448.
48. Chi, W., et al., *Caspase-8 promotes NLRP1/NLRP3 inflammasome activation and IL-1beta production in acute glaucoma.* Proc Natl Acad Sci U S A, 2014. **111**(30): p. 11181-6.
49. Chen, G.Y. and G. Nunez, *Sterile inflammation: sensing and reacting to damage.* Nat Rev Immunol, 2010. **10**(12): p. 826-37.
50. Bergsbaken, T., S.L. Fink, and B.T. Cookson, *Pyroptosis: host cell death and inflammation.* Nat Rev Microbiol, 2009. **7**(2): p. 99-109.
51. Latz, E., T.S. Xiao, and A. Stutz, *Activation and regulation of the inflammasomes.* Nat Rev Immunol, 2013. **13**(6): p. 397-411.
52. Thomas, C.N., et al., *Caspases in retinal ganglion cell death and axon regeneration.* Cell Death Discov, 2017. **3**: p. 17032.
53. Gao, J., et al., *NLRP3 inflammasome: activation and regulation in age-related macular degeneration.* Mediators Inflamm, 2015. **2015**: p. 690243.
54. Song, L., et al., *NLRP3 Inflammasome in Neurological Diseases, from Functions to Therapies.* Front Cell Neurosci, 2017. **11**: p. 63.
55. Bauernfeind, F.G., et al., *Cutting edge: NF-kappaB activating pattern recognition and cytokine receptors license NLRP3 inflammasome activation by regulating NLRP3 expression.* J Immunol, 2009. **183**(2): p. 787-91.
56. Franchi, L., T. Eigenbrod, and G. Nunez, *Cutting edge: TNF-alpha mediates sensitization to ATP and silica via the NLRP3 inflammasome in the absence of microbial stimulation.* J Immunol, 2009. **183**(2): p. 792-6.
57. He, Y., H. Hara, and G. Nunez, *Mechanism and Regulation of NLRP3 Inflammasome Activation.* Trends Biochem Sci, 2016. **41**(12): p. 1012-1021.
58. Bartlett, R., L. Stokes, and R. Sluyter, *The P2X7 receptor channel: recent developments and the use of P2X7 antagonists in models of disease.* Pharmacological reviews, 2014. **66**(3): p. 638-675.

59. Rathkey, J.K., et al., *Live-cell visualization of gasdermin D-driven pyroptotic cell death.* J Biol Chem, 2017. **292**(35): p. 14649-14658.
60. Pandeya, A., et al., *Gasdermin D (GSDMD) as a new target for the treatment of infection.* Medchemcomm, 2019. **10**(5): p. 660-667.
61. Gurung, P. and T.-D. Kanneganti, *Novel roles for caspase-8 in IL-1β and inflammasome regulation.* The American journal of pathology, 2015. **185**(1): p. 17-25.
62. Gurung, P., et al., *FADD and caspase-8 mediate priming and activation of the canonical and noncanonical Nlrp3 inflammasomes.* The Journal of Immunology, 2014. **192**(4): p. 1835-1846.
63. Jha, S., et al., *The inflammasome sensor, NLRP3, regulates CNS inflammation and demyelination via caspase-1 and interleukin-18.* J Neurosci, 2010. **30**(47): p. 15811-20.
64. Guo, H., J.B. Callaway, and J.P. Ting, *Inflammasomes: mechanism of action, role in disease, and therapeutics.* Nat Med, 2015. **21**(7): p. 677-87.
65. Puyang, Z., et al., *Retinal Ganglion Cell Loss is Delayed Following Optic Nerve Crush in NLRP3 Knockout Mice.* Sci Rep, 2016. **6**: p. 20998.
66. Tezel, G. and A.P.O.R.I.C.W.G. Fourth, *The role of glia, mitochondria, and the immune system in glaucoma.* Invest Ophthalmol Vis Sci, 2009. **50**(3): p. 1001-12.
67. Yang, X., et al., *Neurodegenerative and inflammatory pathway components linked to TNF-alpha/TNFR1 signaling in the glaucomatous human retina.* Invest Ophthalmol Vis Sci, 2011. **52**(11): p. 8442-54.
68. Brydges, S.D., et al., *Divergence of IL-1, IL-18, and cell death in NLRP3 inflammasomopathies.* J Clin Invest, 2013. **123**(11): p. 4695-705.
69. Kremer, C.J. and P. Duff, *Glyburide for the treatment of gestational diabetes.* American journal of obstetrics and gynecology, 2004. **190**(5): p. 1438-1439.
70. Lamkanfi, M., et al., *Glyburide inhibits the Cryopyrin/Nalp3 inflammasome.* J Cell Biol, 2009. **187**(1): p. 61-70.
71. Youm, Y.H., et al., *The ketone metabolite beta-hydroxybutyrate blocks NLRP3 inflammasome-mediated inflammatory disease.* Nat Med, 2015. **21**(3): p. 263-9.
72. Jiang, H., et al., *Identification of a selective and direct NLRP3 inhibitor to treat inflammatory disorders.* J Exp Med, 2017. **214**(11): p. 3219-3238.
73. Kuwar, R., et al., *A novel small molecular NLRP3 inflammasome inhibitor alleviates neuroinflammatory response following traumatic brain injury.* J Neuroinflammation, 2019. **16**(1): p. 81.
74. Coll, R.C., et al., *A small-molecule inhibitor of the NLRP3 inflammasome for the treatment of inflammatory diseases.* Nat Med, 2015. **21**(3): p. 248-55.
75. Vande Walle, L., et al., *MCC950/CRID3 potently targets the NACHT domain of wild-type NLRP3 but not disease-associated mutants for inflammasome inhibition.* PLoS Biol, 2019. **17**(9): p. e3000354.
76. Perera, A.P., et al., *MCC950, a specific small molecule inhibitor of NLRP3 inflammasome attenuates colonic inflammation in spontaneous colitis mice.* Sci Rep, 2018. **8**(1): p. 8618.
77. Khan, N., et al., *Pharmacological inhibition of the NLRP3 inflammasome as a potential target for multiple sclerosis induced central neuropathic pain.* Inflammopharmacology, 2018. **26**(1): p. 77-86.

78. LaRock, C.N., et al., *IL-1beta is an innate immune sensor of microbial proteolysis.* Sci Immunol, 2016. **1**(2).
79. Dempsey, C., et al., *Inhibiting the NLRP3 inflammasome with MCC950 promotes non-phlogistic clearance of amyloid-beta and cognitive function in APP/PS1 mice.* Brain Behav Immun, 2017. **61**: p. 306-316.
80. Coates, B.M., et al., *Inhibition of the NOD-Like Receptor Protein 3 Inflammasome Is Protective in Juvenile Influenza A Virus Infection.* Front Immunol, 2017. **8**: p. 782.
81. van Hout, G.P., et al., *The selective NLRP3-inflammasome inhibitor MCC950 reduces infarct size and preserves cardiac function in a pig model of myocardial infarction.* Eur Heart J, 2017. **38**(11): p. 828-836.
82. Simon, W.M., John, et al., *Essential iris atrophy, pigment dispersion, and glaucoma in DBA/2J mice.* Invest Ophthalmol Vis Sci, 1998. **39**.
83. Howell, G.R., et al., *Molecular clustering identifies complement and endothelin induction as early events in a mouse model of glaucoma.* J Clin Invest, 2011. **121**(4): p. 1429-44.
84. A Bouhenni, R., et al., *Animal models of glaucoma.* BioMed Research International, 2012. **2012**.
85. Bo, C., et al., *Interacting loci causes iris atrophy and glaucoma in DBA/2J mice.* Nature Genetics, 1999. **21**.
86. Anderson, M.G., et al., *Mutations in genes encoding melanosomal proteins cause pigmentary glaucoma in DBA/2J mice.* Nat Genet, 2002. **30**(1): p. 81-5.
87. Howell, G.R., et al., *Absence of glaucoma in DBA/2J mice homozygous for wild-type versions of Gpnmb and Tyrp1.* BMC Genet, 2007. **8**: p. 45.
88. John, S.W., M.G. Anderson, and R.S. Smith, *Mouse genetics: a tool to help unlock the mechanisms of glaucoma.* J Glaucoma, 1999. **8**(6): p. 400-12.
89. Mo, J.S., et al., *By altering ocular immune privilege, bone marrow-derived cells pathogenically contribute to DBA/2J pigmentary glaucoma.* J Exp Med, 2003. **197**(10): p. 1335-44.
90. Wong, A.A. and R.E. Brown, *A neurobehavioral analysis of the prevention of visual impairment in the DBA/2J mouse model of glaucoma.* Invest Ophthalmol Vis Sci, 2012. **53**(9): p. 5956-66.
91. Wang, J. and Y. Dong, *Characterization of intraocular pressure pattern and changes of retinal ganglion cells in DBA2J glaucoma mice.* Int J Ophthalmol, 2016. **9**(2): p. 211-7.
92. Bosco, A., et al., *Reduced retina microglial activation and improved optic nerve integrity with minocycline treatment in the DBA/2J mouse model of glaucoma.* Invest Ophthalmol Vis Sci, 2008. **49**(4): p. 1437-46.
93. Wilson, G.N., et al., *Early pro-inflammatory cytokine elevations in the DBA/2J mouse model of glaucoma.* J Neuroinflammation, 2015. **12**: p. 176.
94. Rasmussen, C.A. and P.L. Kaufman, *Primate glaucoma models.* J Glaucoma, 2005. **14**(4): p. 311-4.
95. Pang, I.H. and A.F. Clark, *Rodent models for glaucoma retinopathy and optic neuropathy.* J Glaucoma, 2007. **16**(5): p. 483-505.
96. Gaasterland, D. and C. Kupfer, *Experimental glaucoma in the rhesus monkey.* Invest Ophthalmol, 1974. **13**(6): p. 455-7.
97. Senatorov, V., et al., *Expression of mutated mouse myocilin induces open-angle glaucoma in transgenic mice.* J Neurosci, 2006. **26**(46): p. 11903-14.

98. Mabuchi, F., et al., *Optic nerve damage in mice with a targeted type I collagen mutation.* Invest Ophthalmol Vis Sci, 2004. **45**(6): p. 1841-5.
99. Sawaguchi, K., et al., *Myocilin gene expression in the trabecular meshwork of rats in a steroid-induced ocular hypertension model.* Ophthalmic Res, 2005. **37**(5): p. 235-42.
100. Fujikawa, K., et al., *VAV2 and VAV3 as candidate disease genes for spontaneous glaucoma in mice and humans.* PloS one, 2010. **5**(2): p. e9050.
101. Savinova, O.V., et al., *Intraocular pressure in genetically distinct mice: an update and strain survey.* BMC genetics, 2001. **2**(1): p. 12.
102. Gao, J., et al., *Evidence for the activation of pyroptotic and apoptotic pathways in RPE cells associated with NLRP3 inflammasome in the rodent eye.* Journal of neuroinflammation, 2018. **15**(1): p. 15.
103. Zendedel, A., et al., *Activation and regulation of NLRP3 inflammasome by intrathecal application of SDF-1a in a spinal cord injury model.* Molecular neurobiology, 2016. **53**(5): p. 3063-3075.
104. Cho, M.-H., et al., *Autophagy in microglia degrades extracellular β-amyloid fibrils and regulates the NLRP3 inflammasome.* Autophagy, 2014. **10**(10): p. 1761-1775.
105. Fann, D.Y., et al., *Pathogenesis of acute stroke and the role of inflammasomes.* Ageing Res Rev, 2013. **12**(4): p. 941-66.
106. Yang, F., et al., *NLRP3 deficiency ameliorates neurovascular damage in experimental ischemic stroke.* J Cereb Blood Flow Metab, 2014. **34**(4): p. 660-7.
107. Abulafia, D.P., et al., *Inhibition of the inflammasome complex reduces the inflammatory response after thromboembolic stroke in mice.* J Cereb Blood Flow Metab, 2009. **29**(3): p. 534-44.
108. de Rivero Vaccari, J.P., et al., *A molecular platform in neurons regulates inflammation after spinal cord injury.* J Neurosci, 2008. **28**(13): p. 3404-14.
109. Silverman, W.R., et al., *The pannexin 1 channel activates the inflammasome in neurons and astrocytes.* J Biol Chem, 2009. **284**(27): p. 18143-51.
110. Hong, S., et al., *Isolation of primary mouse retinal ganglion cells using immunopanning-magnetic separation.* Molecular vision, 2012. **18**: p. 2922.
111. Mo, J.-S., W. Wang, and H.J. Kaplan, *Impact of inflammation on ocular immune privilege.* Chemical immunology and allergy, 2007. **92**: p. 155.
112. Jiang, H.R., et al., *IL-18 not required for IRBP peptide-induced EAU: studies in gene-deficient mice.* Invest Ophthalmol Vis Sci, 2001. **42**(1): p. 177-82.
113. Zhou, X., et al., *Involvement of inflammation, degradation, and apoptosis in a mouse model of glaucoma.* J Biol Chem, 2005. **280**(35): p. 31240-8.
114. Kesav, N., et al., *Current Management of Uveitis-associated Ocular Hypertension and Glaucoma.* Surv Ophthalmol, 2019.
115. Toris, C.B., *Aqueous humor dynamics I: measurement methods and animal studies.* Current Topics in Membranes, 2008. **62**: p. 193-229.
116. Takahashi, T., et al., *A clinical evaluation of uveitis-associated secondary glaucoma.* Japanese journal of ophthalmology, 2002. **46**(5): p. 556-562.
117. Chi, W., et al., *HMGB1 promotes the activation of NLRP3 and caspase-8 inflammasomes via NF-kappaB pathway in acute glaucoma.* J Neuroinflammation, 2015. **12**: p. 137.
118. Reichstein, D., et al., *Apoptotic retinal ganglion cell death in the DBA/2 mouse model of glaucoma.* Exp Eye Res, 2007. **84**(1): p. 13-21.

119. Wei, X., et al., *Neuroinflammation and microglia in glaucoma: time for a paradigm shift.* J Neurosci Res, 2019. **97**(1): p. 70-76.
120. Frank, M.G., et al., *The redox state of the alarmin HMGB1 is a pivotal factor in neuroinflammatory and microglial priming: a role for the NLRP3 inflammasome.* Brain, behavior, and immunity, 2016. **55**: p. 215-224.

Appendix

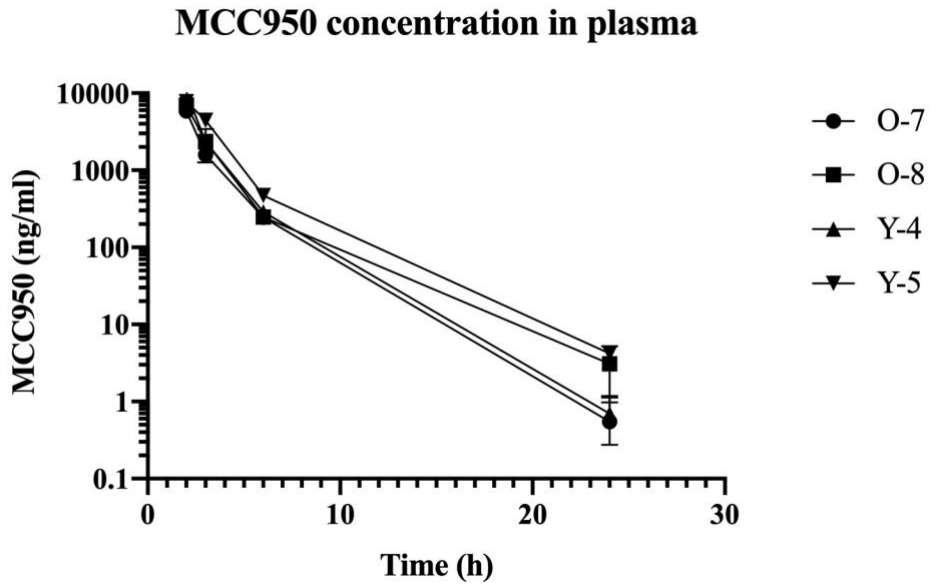

Figure A-1. Pilot study of pharmacokinetic analysis of MCC950. Four animals are used in the metabolism study, with two 3-month mice (Y-4, Y-5) and two 9-month mice (O-8, O-9) respectively. MCC950 concentration was measured at a series of time point after intraperitoneal injection of 20mg/kg. As the pharmacokinetic result suggested, MCC950 concentration ranged from 5844 ng/ml to 10389 ng/ml at 1 hour after injection and decreased dramatically to 245-470 ng/ml 6 hours post injection. At 24 hours post injection, the concentration decreased below 5 ng/ml.